# Indole produced during dysbiosis mediates host–microorganism chemical communication

Rui-Qiu Yang[1,*], Yong-Hong Chen[1,*], Qin-Yi Wu[2*], Jie Tang[1,3*], Shan-Zhuang Niu[1], Qiu Zhao[1], Yi-Cheng Ma[1,#], and Cheng-Gang Zou [1,#]

[1] State key Laboratory for Conservation and Utilization of Bio-Resources in Yunnan, School of Life Sciences, Yunnan University, Kunming, Yunnan 650091, China. [2] Yunnan Provincial Key Laboratory of Molecular Biology for Sinomedicine, Yunnan University of Chinese Medicine, Kunming 650500, Yunnan, China. [3] Yunnan Key Laboratory of Vaccine Research Development on Severe Infectious Disease, Institute of Medical Biology, Chinese Academy of Medical Sciences and Peking Union Medical College, Kunming 650118, China.

*These authors contributed equally to this work.

[#]Correspondence and requests for materials should be addressed to Y.-C.M. (email: mayc@ynu.edu.cn), or C.-G. Z. (email: chgzou@ynu.edu.cn).

**Abstract**

An imbalance of the gut microbiota, termed dysbiosis, has a substantial impact on host physiology. However, the mechanism by which host deals with gut dysbiosis to maintain fitness remains largely unknown. In *C. elegans*, *E. coli*, which is its bacterial diets, proliferates in its intestinal lumen during aging. Here, we demonstrate that progressive intestinal proliferation of *E. coli* activates the transcription factor DAF-16, which is required for maintenance of longevity and organismal fitness in worms with age. DAF-16 up-regulates two lysozymes *lys-7* and *lys-8*, thus limiting the bacterial accumulation in the gut of worms during aging. During dysbiosis, the levels of indole produced by *E. coli* are increased in worms. Indole is involved in the activation of DAF-16 by TRPA-1 in neurons of worms. Our finding demonstrates that indole functions as a microbial signal of gut dysbiosis to promote fitness of the host.

## Introduction

The microbiota in the gut has a substantial impact on host nutrition, metabolism, immune function, development, behavior, and lifespan (Lee & Brey 2013; Johnson & Foster 2018; Bana & Cabreiro 2019). Microbial community disequilibria, so-called dysbiosis, has been implicated in a broad range of human diseases, such as obesity, insulin resistance, autoimmune disorders, inflammatory bowel disease (IBD), aging and increased pathogen susceptibility (Honda & Littman 2012; Wu *et al.* 2015). Therefore, understanding of the mechanisms that modulate host–microbe interactions will provide important insight into treating these diseases by intervening the microbial communities.

The genetically tractable model organism *Caenorhabditis elegans* has contributed greatly to understand the role of host-microbiota interactions in host physiology (Cabreiro & Gems 2013; Zhang *et al.* 2017). In the bacterivore nematode, the microbiota in the gut can be easily manipulated, making it an excellent model for studying how the microbiota affect host physiology in the context of disease and aging at a single species (Cabreiro & Gems 2013). For instance, the neurotransmitter tyramine produced by intestinal Providencia bacteria can direct sensory behavioural decisions by modulate multiple monoaminergic pathways in *C. elegans* (O'Donnell *et al.* 2020). On the other hand, *C. elegans*-based studies have revealed a variety of signaling cascades involved in the innate immune responses against microbial infection (Irazoqui *et al.* 2010b), including the p38 mitogen activated protein kinase (MAPK)/PMK-1, ERK MAPK/MPK-1, the heat shock transcription factor HSF-1, the transforming growth factor (TGF)β/bone morphogenetic protein (BMP) signaling (Zugasti & Ewbank 2009), and the forkhead transcription factor DAF-16/FOXO pathway (Kim *et al.*

2002; Garsin *et al.* 2003; Singh & Aballay 2006; Zou *et al.* 2013). In Drosophila and mammalian cells, activation of FOXOs up-regulates a set of antimicrobial peptides, such as drosomycin and defensins (Becker *et al.* 2010), implicating that the role for FOXOs in innate immunity is conserved across species. Furthermore, disruption of these innate immune-reltaed pathways, such as the p38 MAPK pathway and the TGFβ/BMP signaling cascade, turns beneficial bacteria commensal to pathogenic in worms (Montalvo-Katz *et al.* 2013; Berg *et al.* 2019). These results indicate that the integrity of immune system is also essential for host defense against non-pathogenic bacteria.

*Escherichia coli* (strain OP50) is conventionally used as a bacterial food for culturing *C. elegans*. In general, most of *E. coli* is efficiently disrupted by a muscular grinder in the pharynx of the worm. However, very few intact bacteria may escape from this defense system, and enter in the lumen of the worm intestine (Gupta & Singh 2017). The intestinal lumen of worms is frequently distended during aging, which accompanied by bacterial proliferation (Garigan *et al.* 2002; McGee *et al.* 2011). Blockage of bacterial proliferation by treatment of UV, antibiotics, and heat extends lifespan of worms (Garigan *et al.* 2002; De Arras *et al.* 2014; Hwang *et al.* 2014), implicating that progressive intestinal proliferation of *E. coli* probably contributes to worm aging and death. Thus, age-related dysbiosis in *C. elegans* provides a model to study how host responses to altered gut microbiota to maintain fitness (Ezcurra 2018).

Accumulating evidence has indicated that genetic inactivation of *daf-16* accelerates tissue deterioration and shortens lifespan of wild-type (WT) worms grown on *E. coli* OP50 (Garigan *et al.* 2002; Portal-Celhay & Blaser 2012; Portal-Celhay *et al.* 2012; Li *et al.* 2019).

The observation that DAF-16 is activated during bacterial accumulation in older worms (Li *et al.* 2019), prompt us to investigate the role of DAF-16 in dysbiosis in the gut of worms. We found that activation of DAF-16 was required for maintenance of longevity and organismal fitness in worms, at least in part, by up-regulating two lysozyme genes (*lys-7* and *lys-8*), thus limiting bacterial accumulation in the gut of worms during aging. Meanwhile, we identified that indole produced by *E. coli* was involved in the activation of DAF-16 by TRPA-1.

## Results

### Activation of DAF-16 is required for normal lifespan and organismal fitness in worms.

To study the role of DAF-16 in age-related dysbiosis, all the experiments started from the young adult stage, which was considered Day 0 (0 days) (Figure 1-figure supplement 1A). Consistent with a recent observation that DAF-16 is activated in worms with age (Li *et al.* 2019), we found that DAF-16::GFP was mainly located in the cytoplasm of the intestine in worms expressing *daf-16p::daf-16::gfp* fed live *E. coli* OP50 on Day 1 (Figure 1A and 1B). The nuclear translocation of DAF-16 in the intestine was increased in worms fed live *E. coli* OP50 on Days 4 and 7, but not in age-matched WT worms fed heat-killed (HK) *E. coli* OP50 (Figure 1A and 1B). To further confirm these results, we tested the expression of two DAF-16 target genes *dod-3* and *hsp-16.2* via the transcriptional reporter strains of *dod-3p::gfp* and *hsp-16.2p::nCherry*. As expected, the expression of either *dod-3p::gfp* or *hsp-16.2p::nCherry* was significantly up-regulated in worms fed live *E. coli* OP50 on Day 4, but not in age-matched worms fed HK *E. coli* OP50 (Figure 1-figure supplement 1B-1D). Likewise, DAF-16 was also retained in the cytoplasm of the intestine in worms fed ampicillin-killed *E.*

111 *coli* OP50 on Days 4 and 7 (Figure 1-figure supplement 2A). In contrast, starvation induced
112 the nuclear translocation of DAF-16 in the intestine of worms on Day 1 (Figure 1-figure
113 supplement 2B). Thus, either HK or antibiotic-killed *E. coli* OP50 as a food source does not
114 induce a starvation state in worms. Taken together, these results indicate that activation of
115 DAF-16 is mainly attributed to accumulation of live *E. coli*, but not by age itself, in worms.

116 Consistent with the previous observations (Portal-Celhay *et al.* 2012; Li *et al.* 2019), we
117 found that a mutation in *daf-16(mu86)* shortened lifespan of worms fed live *E. coli* OP50 at
118 20 °C (Figure 1C). In contrast, the mutation in *daf-16(mu86)* had no impact on lifespan of
119 worms fed either HK (Figure 1C) or ampicillin-killed *E. coli* OP50 (Figure 1-figure
120 supplement 2C). Next, we examined the effects of DAF-16 on phenotypic traits, such as the
121 pharyngeal-pumping rate, body bending, and integrity of intestinal barrier, which are
122 associated with aging in worms. Both the rates of pharyngeal-pumping (Figure 1D) and body
123 bending (Figure 1E) were reduced in *daf-16(mu86)* mutants on Day 7 as compared to those in
124 WT worms fed live *E. coli* OP50. In contrast, the rates of pharyngeal-pumping and body
125 bending were comparable in WT worms and *daf-16(mu86)* mutants grown on HK *E. coli*
126 OP50 on Day 7. Furthermore, we used food dye FD&C Blue No. 1 to evaluate the integrity of
127 intestinal barrier (Ma *et al.* 2020). The body-cavity leakage in *daf-16(mu86)* mutants on Days
128 7 and 10 were higher than those in age-matched WT worms fed live *E. coli* OP50, but not HK
129 *E. coli* OP50 (Figure 1F and 1G). Taken together, these results demonstrate that activation of
130 DAF-16 by bacterial accumulation is required for maintenance of longevity and organismal
131 fitness.

132

## Indole produced from *E. coli* activates DAF-16

As DAF-16 is activated by bacterial accumulation, we hypothesized that this activation is probably due to bacterially produced compounds. To test this idea, culture supernatants from *E. coli* OP50 were collected, and freeze-dried. After dissolved in methanol, the crude extract was isolated by high performance liquid chromatograph (HPLC) with automated fraction collector using Agilent ZORBAX SB-C18 liquid chromatography column. A candidate compound was detected by activity-guided isolation, and further identified as indole with mass spectrometry and NMR data (Figure 2A, Figure 2-figure supplement 1A and 1B; Table S1). The observation that indole secreted by *E. coli* OP50 could activate DAF-16 was further confirmed by analyzing commercial HPLC grade indole. Supplementation with indole (50-200 μM) not only significantly induced nuclear translocation of DAF-16 (Figure 2B), but also up-regulated the expression of either *dod-3p::gfp* or *hsp-16.2p::nCherry* in young adult worms after 24 h of treatment (Figure 2-figure supplement 2A and 2B). Next, we found that the levels of indole were 30.9, 71.9, and 105.9 nmol/g dry weight, respectively, in worms fed live *E. coli* OP50 on Days 1, 4, and 7 (Figure 2C). The elevated indole levels in worms were accompanied by an increase in colony-forming units (CFU) of live *E. coli* OP50 in the intestine of worms with age (Figure 2C), suggesting that accumulation of live *E. coli* OP50 in the intestine is probably responsible for increased indole in worms. These data also raised a possibility that exogenous indole produced by *E. coli* OP50 on the NGM plates could increase the levels of indole in worms with age. However, we found that the levels of indole were 28.2, 31.6, and 36.1 nmol/g dry weight, respectively, in worms fed HK *E. coli* OP50 on Days 1, 4, and 7 (Figure 2-figure supplement 3A), indicating that indole was not accumulated in worms

fed HK *E. coli* OP50 even for 7 days. Thus, the increase in the levels of indole in worms results from intestinal accumulation of live *E. coli* OP50, rather than exogenous indole produced by *E. coli* OP50 on the NGM plates. The observation that DAF-16 was retained in the cytoplasm of the intestine in worms fed live *E. coli* OP50 on Day 1 (Figure 1A and 1B) also indicated that exogenous indole produced by *E. coli* OP50 on the NGM plates is not enough to activate DAF-16. Supplementation with indole (50-200 μM) significantly increased the indole levels in young adult worms on Day 1 (Figure 2-figure supplement 3B), which could induce nuclear translocation of DAF-16 in worms (Figure 2B).

In bacteria, indole is biosynthesized from tryptophan by tryptophanase (*tnaA*) (Lee *et al.* 2015). To determine the effect of endogenous indole, worms were fed *E. coli* K-12 BW25113 strain (called K-12), and *tnaA*-deficient strain BW25113 *ΔtnaA* (called K-12 *ΔtnaA*), respectively. We found that both *tnaA* mRNA and indole levels were undetectable in the K-12 *⊿tnaA* strain (Figure 2-figure supplement 4A and 4B). Furthermore, disruption of *tnaA* significantly suppressed the nuclear translocation of DAF-16 (Figure 2D). The nuclear translocation of DAF-16::GFP was mainly located in the cytoplasm of the intestine in worms fed live K-12 *⊿tnaA* strains on Day 4. However, supplementation with indole induced the nuclear translocation of DAF-16::GFP in the intestine in these worms (Figure 2-figure supplement 4C). Taken together, our results suggest that indole is involved in the activation of DAF-16 in worms with age.

**Endogenous indole is required for normal lifespan**

It has been shown that exogenous indole extends lifespan in *C. elegans* at 16 °C (Sonowal *et*

177 *al.* 2017). We found that adult worms fed *E. coli* K-12 *ΔtnaA* strains exhibited a shortened
178 lifespan at 20 °C, compared with those fed *E. coli* K-12 strain (Figure 3A). Supplementation
179 with indole in adults not only rescued the shortened lifespan of WT worms fed *E. coli* K-12
180 *ΔtnaA* strain, but also significantly extended the lifespan of WT worms fed *E. coli* K-12 strain
181 (Figure 3A). In contrast, the lifespan of *daf-16(mu86)* mutants fed *E. coli* K-12 *ΔtnaA* strain
182 was comparable to that of *daf-16(mu86)* mutants fed *E. coli* K-12 strain (Figure 3B).
183 Supplementation with indole (100 μM) did not affect the lifespan of *daf-16(mu86)* mutants
184 fed either *E. coli* K-12 or K-12 *ΔtnaA* strain (Figure 3B). Moreover, the CFU of *E. coli* K-12
185 *ΔtnaA* strain were significantly higher than those of *E. coli* K12 strain in WT worms on Days
186 4 and 7 (Figure 3C). By contrast, the CFU of *E. coli* K-12 *ΔtnaA* strain were similar to those
187 of *E. coli* K12 strain in *daf-16(mu86)* mutants on Days 4 and 7 (Figure 3D). Likewise, the
188 accumulation of *E. coli* K-12 *ΔtnaA* strain expressing mCherry were significantly higher than
189 that of *E. coli* K12 strain in WT worms, but not *daf-16(mu86)* mutants, on Days 4 and 7
190 (Figure 3E-3G). Finally, supplementation with indole (100 μM) inhibited the CFU of *E. coli*
191 K-12 in WT worms, but not *daf-16(mu86)* mutants, on Days 4 and 7 (Figure 3H and 3I).
192 These results suggest that endogenous indole is involved in maintaining normal lifespan in
193 worms.
194
195 **TRPA-1 in neurons is required for indole-mediated longevity**
196 How did worms detect bacterially produced indole during aging? Previously, Sonowal et al.
197 have identified that *C. elegans* xenobiotic receptor AHR-1, which encodes an ortholog of the
198 mammalian AHR, mediates indole-promoted lifespan extension in worms at 16 °C (Sonowal

199 *et al.* 2017). However, we found that RNAi knockdown of *ahr-1* did not affect the nuclear
200 translocation of DAF-16 in worms fed *E. coli* K12 strain on Day 7 (Figure 4-figure
201 supplement 1A) or young adult worms treated with indole (100 μM) for 24 h (Figure 4-figure
202 supplement 1B). A recent study has demonstrated that bacteria-derived indole activates the
203 transient receptor potential ankyrin 1 (TRPA1), a cold-sensitive TRP channel, in
204 enteroendocrine cells in zebrafish and mammals (Ye *et al.* 2021). As *C. elegans* TRPA-1 is an
205 ortholog of mammalian TRPA1 (Kindt *et al.* 2007; Venkatachalam & Montell 2007), we
206 tested the role of TRPA-1 in DAF-16 activation by indole. We found that RNAi knockdown
207 of *trpa-1* significantly inhibited the nuclear translocation of DAF-16 in worms fed *E. coli* K12
208 strain on Days 4 and 7 (Figure 4A) or young adult worms treated with indole (100 μM) for 24
209 h (Figure 4B). These results suggest that TRPA-1 is involved in indole-mediated DAF-16
210 activation. Previously, Xiao et al. (Xiao *et al.* 2013) have demonstrated that TRPA-1 activated
211 by low temperatures mediates calcium influx, which in turn stimulates the PKC-2-SGK-1
212 signaling to promote the transcription activity of DAF-16, leading to lifespan extension in
213 worms. However, we found that RNAi knockdown of *sgk-1* did not influence the
214 nucleocytoplasmic distribution of DAF-16 in the presence of indole (Figure 4-figure
215 supplement 1C). Mutant worms lacking *trpa-1* exhibited a shorter lifespan than did WT
216 worms at 20 °C (Xiao *et al.* 2013). Consistent with this observation, knockdown of *trpa-1* by
217 RNAi significantly shortened the lifespan in worms fed *E. coli* K12 strain (Figure 4C).
218 Supplementation with indole no longer extended the lifespan of worms after knockdown of
219 *trpa-1* by RNAi. Furthermore, the CFU of *E. coli* K-12 strain were significantly increased in
220 worms subjected to *trpa-1* RNAi on Days 4 and 7 (Figure 4D and 4E). Supplementation with

indole failed to suppress the increases in CFU in these worms. These results suggest that indole exhibits its function in extending lifespan and inhibiting bacterial accumulation primarily via TRPA-1. It has been shown that podocarpic acid, a TRPA-1 agonist, activates the SEK-1/PMK-1/SKN-1 pathway (Chaudhuri *et al.* 2016), a signaling cascade involved in *C. elegans* defense against pathogenic bacteria (Kim *et al.* 2002). However, we found that supplementation with 0.1 mM indole failed to induce nuclear localization of SKN-1::GFP in the intestine of the transgenic worms expressing *skn-1p::skn-1::gfp* (Figure 4-figure supplement 2A and 2B), suggesting that indole cannot activate SKN-1 in worms.

As overexpression of *trpa-1* in the intestine and neurons was sufficient to extend the lifespan of worms (Xiao *et al.* 2013), we determined tissue-specific activities of TRPA-1 in the regulation of longevity mediated by indole. Consistent with this observation (Xiao *et al.* 2013), we found that both neuronal- and intestinal-specific knockdown of *trpa-1* by RNAi significantly shortened the lifespans in worms (Figure 5A and 5B). However, supplementation with indole (100 μM) only extended the lifespan in worms subjected to intestinal-specific (Figure 5B), but not neuronal-specific, *trpa-1* RNAi (Figure 5A). Likewise, knockdown of *trpa-1* in either neurons (Figure 5C and 5D) or the intestine (Figure 5E and 5F) increased the CFU of *E. coli* K-12 in worms on Days 4 and 7. However, supplementation with indole failed to inhibit the increase in the CFU of *E. coli* K-12 in worms subjected to neuronal-specific *trpa-1* RNAi (Figure 5C and 5D). By contrast, supplementation with indole significantly suppressed the CFU of *E. coli* K-12 in these worms subjected to intestinal-specific *trpa-1* RNAi (Figure 5E and 5F). These results suggest that TRPA-1 in neurons is involved in indole-mediated longevity.

**LYS-7 and LYS-8 functions as downstream molecules of DAF-16 to maintain normal lifespan in worms**

*C. elegans* possesses a variety of putative antimicrobial effector proteins, such as lysozymes, defensin-like peptides, neuropeptide-like proteins, and caenacins (Dierking *et al.* 2016). Of these antimicrobial proteins, *C. elegans* lysozymes are involved in host defense against various pathogens (Mallo *et al.* 2002; O'Rourke *et al.* 2006; Irazoqui *et al.* 2010a; Boehnisch *et al.* 2011; Visvikis *et al.* 2014). A previous study has demonstrated that expressions of lysozyme genes, such as *lys-2, lys-7,* and *lys-8,* are markedly up-regulated in 4-day-old worms, which is dependent on DAF-16 (Li *et al.* 2019). We thus determined the role of these lysozyme genes in lifespan of worms. We found that a single mutation in *lys-7(ok1384)* slightly but significantly reduced the lifespan in worms fed live *E. coli* OP50 (Figure 6-figure supplement 1A), but not HK *E. coli* OP50 (Figure 6-figure supplement 1B), which was consistent with a previous observation (Portal-Celhay *et al.* 2012). In contrast, whereas either a single mutation in *lys-8(ok3504)* or RNAi knockdown of *lys-2* did not affect the lifespan in worms grown on live *E. coli* OP50, or HK *E. coli* OP50 (Figure 6-figure supplement 1A and 1B). However, *lys-7(ok1384); lys-8(ok3504)* double mutants exhibited a shortened lifespan in worms fed live *E. coli* OP50 (Figure 6A). In contrast, the lifespan of *lys-7(ok1384); lys-8(ok3504)* double mutants was comparable to that of WT worms fed HK *E. coli* OP50 (Figure 6B). Furthermore, knockdown of *lys-2* by RNAi did not affect the lifespan of *lys-7(ok1384); lys-8(ok3504)* double mutants grown on live *E. coli* OP50, or HK *E. coli* OP50 (Figure 6-figure supplement 1C and 1D). Both the rates of pharyngeal-pumping (Figure 6C)

and body bending (Figure 6D) were reduced in 8-day-old *lys-7(ok1384); lys-8(ok3504)* double mutants fed live *E. coli* OP50. Moreover, the body-cavity leakage was increased in the double mutants fed live *E. coli* OP50 on Day 10 (Figure 6E). However, these age-associated markers in *lys-7(ok1384); lys-8(ok3504)* double mutants were comparable to those in in age-matched WT worms fed HK *E. coli* OP50. In addition, we found that double mutations in *lys-7(ok1384); lys-8(ok3504)* increased the CFU of *E. coli* OP50 (Figure 6F) as well as accumulation of *E. coli* OP50 expressing RFP in worms on Day 7 (Figure 6G). Finally, we found that supplementation with indole no longer extended lifespan and failed to suppress the increase the CFU of *E. coli* K-12 in *lys-7(ok1384); lys-8(ok3504)* double mutants (Figure 6-figure supplement 2A and 2B).

Using the transgenic worms expressing either *lys-7p::gfp* or *lys-8p::gfp*, we found that the expressions of *lys-7p::gfp* and *lys-8p::gfp* were significantly up-regulated in worms fed live *E. coli* OP50 on Days 4 and 7 (Figure 7-figure supplement 1A-1D), but not in age-matched worms fed HK *E. coli* OP50 (Figure 7-figure supplement 1A-1D). RNAi knockdown of *daf-16* also significantly suppressed the expressions of *lys-7p::gfp* and *lys-8p::gfp* in these worms fed live *E. coli* OP50 (Figure 7A and 7B). Similar results were obtained by measuring the mRNA levels of *lys-7* and *lys-8* in *daf-16(mu86)* mutants using quantitive real-time PCR (qPCR) (Figure S11E and S11F). Furthermore, we found that expression of either *lys-7p::gfp* (Figure 7C) or *lys-8p::gfp* (Figure 7D) was reduced in worms fed *E. coli* K-12 *ΔtnaA* strain on Days 4 and 7, compared to those in age-matched worms fed *E. coli* K-12 strain. Likewise, indole (100 μM) remarkably increased the expression of either *lys-7p::gfp* or *lys-8::gfp* in young adult worms after 24 h treatment (Figure 7E and 7F).

Finally, we found that RNAi knockdown of *trpa-1* significantly inhibited the expression of either *lys-7p::gfp* or *lys-8p::gfp* in 4-day-old worms fed *E. coli* K12 strain (Figure 7A and 7B). Meanwhile, we found that the mRNA levels of *lys-7* and *lys-8* were significantly down-regulated in worms subjected to neuronal-specific (Figure 7-figure supplement 2A), but not intestinal-specific, knockdown of *trpa-1* by RNAi on Day 4 (Figure 7-figure supplement 2B). However, supplementation with indole only up-regulated the expression of *lys-7* and *lys-8* in worms subjected to intestinal-specific (Figure 7-figure supplement 2C), but not neuronal-specific, RNAi of *trpa-1* (Figure 7-figure supplement 2D). These results suggest that LYS-7 and LYS-8 function as downstream molecules of DAF-16 to maintain normal lifespan by inhibiting bacterial proliferation in worms.

## Discussion

Using *C. elegans* and its dietary bacterium as a host-microbe model, we provide a striking example of how a host responds to microbial dysbiosis in the gut. As worms age, *E. coli* proliferates in the lumen, thereby producing and secreting more indole. When its concentration crosses a threshold value, the bacterially produced compound is perceived by TRPA-1 in worms. The TRPA-1 signaling triggers DAF-16 nuclear translocation, leading to up-regulation of lysozyme genes. These antimicrobial peptides help worms to maintain normal lifespan by limiting the bacterial proliferation.

A complication in understanding the impact of bacterial diets on the traits of the worm is the fact that initially bacteria are a source of food, but later become pathogenic (Garigan *et al.* 2002; Tan & Shapira 2011). Thus, the accumulation of *E. coli* in the gut is harmful for

organismal fitness of worms during the course of life. As a well-known regulator of longevity and innate immunity (Garsin *et al.* 2003; Zou *et al.* 2013), DAF-16 is activated in aging *C. elegans* (Li *et al.* 2019). This transcription factor is involved in both maintaining normal lifespan and limiting proliferation of *E. coli* in worms (Garigan *et al.* 2002; Portal-Celhay & Blaser 2012; Portal-Celhay *et al.* 2012). In this study, our data demonstrate that activation of DAF-16 requires contact with live bacterial cells in the gut of worms as dead *E. coli* fails to activate DAF-16. Thus, accumulation of *E. coli* during aging, but not aging itself, results in the activation of DAF-16. Furthermore, DAF-16 mutation does not influence the lifespan in worms fed dead *E. coli*. Taken together, these findings clearly demonstrate that DAF-16 acts to maintain homeostasis by inhibiting bacterial proliferation in worms with age.

Indole is produced from tryptophan by tryptophanase in a large number of bacterial species. As a well-known signaling molecule, indole is involved in regulation of a variety of physiological processes in bacteria, such as cell division, biofilm formation, virulence, spore formation, and antibiotic resistance (Lee *et al.* 2015; Zarkan *et al.* 2020). Although animals cannot synthesize indole, they can sense and modify this metabolite (Lee *et al.* 2015). Indole and its derivatives can influence insect behaviors and human diseases, such as intestinal inflammation and diabetes (Lee *et al.* 2015; Agus *et al.* 2018). Thus, indole may function as an interspecies and interkingdom signaling molecule to influence the microbe-host interaction (Bansal *et al.* 2010; Oh *et al.* 2012; Ye *et al.* 2021). For instance, enteric delivery of indole (1 mM) increases intestinal motility by inducing 5-hydroxytryptamine secretion in zebrafish larvae (Ye *et al.* 2021). Supplementation with 0.2 mM indole enhances the resistance of *C. elegans* to infection with *C. albicans* by reducing fungal colonization in the intestine (Oh *et al.*

2012). In addition, treatment of HCT-8 intestinal epithelial cells with 1 mM indole inhibits TNF-α-mediated activation of NF-κB and up-regulation of the inflammatory factor IL-8, thus improving intestinal epithelial barrier function (Bansal *et al.* 2010). Our data show that indole limits the bacterial proliferation in the gut of worms by driving intestinal defense gene expression via the transcription factor DAF-16. These findings suggest that the bacteria-derived metabolite may serve as a pathogen-associated molecular pattern that is recognized by metazoans. Although it has been shown that indole at a higher concentration (5 mM) is capable of inhibiting cell division in *E. coli* K12 strain (Chimerel *et al.* 2012), exogenous indole has little effect on the growth of *E. coli* K12 strain up to 3 mM (Chant & Summers 2007). In general, extracellular indole concentrations detected in stationary phase LB cultures are typically 0.5-1 mM depending on the specific *E. coli* strain (Zarkan *et al.* 2020). Our data show that indole is sufficient to inhibit accumulation of *E. coli* BW25113 with the concentration range from 0.05-0.2 mM. Thus, these results suggest that direct causal involvement of cell cycle arrest in *E. coli* by indole is unlikely.

Our data demonstrate that the cold-sensitive TRP channel TRPA-1 in neurons is involved in indole-mediated nuclear translocation of DAF-16 in the intestine, which is required for lifespan extension in *C. elegans*. *trpa-1* is widely expressed in a variety of sensory neurons in worms (Kindt *et al.* 2007). One possibility is that TRPA-1 in neurons may release a neuropeptide, which in turn triggers a signaling pathway to extend lifespan of worms via activating DAF-16 in a non-cell autonomous manner. Low temperature also activates TRPA-1, which in turn acts to promote longevity via the PKC-2-SKG-1-DAF-16 pathway (Xiao *et al.* 2013). It should be noted that unlike indole, activation of TPRA-1 by low temperature

353 promotes the transcription activity, but not the nuclear translocation, of DAF-16 (Xiao *et al.*
354 2013). Furthermore, our data show that knockdown of *sgk-1* dose not influence the nuclear
355 translocation of DAF-16 induced by indole. Finally, indole extends lifespan via TRPA-1 only
356 in nervous system, whereas low temperature extends lifespan via TRPA-1 both in the intestine
357 and neurons. Thus, indole-mediated lifespan extension is essentially different from low
358 temperature-mediated lifespan extension, although TRPA-1 and DAF-16 are involved in both
359 processes. Although podocarpic acid, the agonist of TRPA-1, can activate the TRPA-1-SKN-1
360 pathway, SKN-1 is unlikely to be involved in indole-mediated biological effects. We observe
361 that indole fails to activate SKN-1 in worms. More importantly, podocarpic acid does not
362 affect the lifespan in worms (Chaudhuri *et al.* 2016). These data implicate that TRPA-1
363 activation via indole and via podocarpic acid happens through distinct mechanisms.

364 In this study, our data demonstrate that DAF-16 inhibits bacterial proliferation by
365 up-regulating expression of two lysozyme genes, *lys-7* and *lys-8*. As a group of digestive
366 enzymes with antimicrobial properties, lysozymes play an important role in the innate
367 immunity in both vertebrate and invertebrate animals (O'Rourke *et al.* 2006). As a target gene
368 of DAF-16, *lys-7* has been proven to play an important role in resistance against a variety of
369 pathogens, such as *Microbacterium nematophilum* (O'Rourke *et al.* 2006), *Pseudomonas*
370 *aeruginosa* (Nandakumar & Tan 2008), the pathogenic *E. coli* LF82 (Simonsen *et al.* 2011),
371 *Bacillus thuringiensis* (Boehnisch *et al.* 2011), and *Cryptococcus neoformans* (Marsh *et al.*
372 2011). A previous study has demonstrated that a mutation in *lys-7* significantly reduces
373 lifespan, but does not influence the accumulation of *E. coli* OP50 in the intestine of
374 2-days-old worms (Portal-Celhay *et al.* 2012). In the current study, the *lys-7* mutants exhibit

reduced lifespan and elevated bacterial loads in the intestine of worms on Days 4 and 7. This discrepancy may be due to the different worms at different ages. Actually, our data also show that the *lys-7;lys-8* double mutants exhibit a comparable accumulation of *E. coli* OP50 in worms on Day 1. Although *lys-8* mutation dose not influence either lifespan or bacterial loads, it enhances the effect of *lys-7*. These results suggest that *lys-8* acts in synergy with *lys-7* to limit bacterial accumulation in the gut of worms.

It has been well established that bacterial dysbiosis is significantly associated with inflammatory bowel diseases (IBD) (Manichanh *et al.* 2012; Sommer & Backhed 2013). Interestingly, reduced levels of indole and its derivative indole-3-propionic acid (IPA) are observed in serum of mice with dextran sulfate sodium-induced colitis and patients with IBD (Alexeev *et al.* 2018). Oral administration of IPA significantly ameliorates disease and promotes intestinal homeostasis by up-regulating colonic epithelial IL-10R1 in the chemically induced murine colitis model. Thus, characterization of the role for indole and its derivatives in host–microbiota interactions within the mucosa may provide new therapeutic avenues for inflammatory intestinal diseases.

## Materials and Methods

**Nematode strains.** *daf-16(mu86)*, *lys-7(ok1384)*, *lys-8(ok3504)*, LD1*[skn-1b/c::gfp + rol-6(su1006)]*, the nematode strain for neuronal-specific RNAi, TU3401 (*sid-1(pk3321); uIs69 [pCFJ90 (myo-2p:: mCherry) + unc-119p::sid-1]*), TJ356 *(zIs356 [daf-16p::daf-16a/b::GFP + rol-6 (su1006)]*), SAL105 (*denEx2 [lys-7::GFP + pha-1(+)]*) were kindly provided by the Caenorhabditis Genetics Center (CGC;

http://www.cbs.umn.edu/CGC), funded by NIH Office of Research Infrastructure Programs (P40 OD010440). The nematode strain for intestinal-specific RNAi, MGH170 (*sid-1(qt9); Is[vha-6pr::sid-1]; Is[sur-5pr::GFPNLS*]), was kindly provided by Dr. Gary Ruvkun (Massachusetts General Hospital, Harvard Medical School). The strain MQD1586 (*476*[*hsp-16.2p::nCherry*; *dod-3p::gfp*; *mtl-1::bfp*, *unc-119(+)]*) was kindly provided by Dr. Mengqiu Dong (Beijing Institute of Life Sciences). Mutants were backcrossed three times into the N2 strain used in the laboratory. All strains were maintained on nematode growth media (NGM) and fed with *E. coli* OP50 at 20 ℃.

**Study Design for age-related dysbiosis study.** Synchronized L1 larvae were grown on NGM agar plates seeded with *E. coli* OP50 at 20 ℃ until they reached the young adult stage. All the experiments started from the young adult stage, which was considered Day 0 (0 days). From Day 1 to Day 10, the worms were transferred to new NGM plates containing *E. coli* strains at 20 ˚C daily for further experiments. BW21153 (*E. coli* K-12 wild-type) and *E. coli* K-12 *ΔtnaA* strain were obtained from the Keio collection (Baba *et al.* 2006).

**RNA interference.** RNAi bacterial strains containing targeting genes were obtained from the Ahringer RNAi library (Kamath & Ahringer 2003). All clones used in this study were verified by sequencing. Briefly, *E. coli* strain HT115 (DE3) expressing dsRNA was grown in LB (Luria-Bertani) containing 100 μg/ml ampicillin at 37 ℃ for overnight, and then spread onto NGM plates containing 100 μg/ml ampicillin and 5 mM isopropyl 1-thio-β-D-galactopyranoside (IPTG). The RNAi-expressing bacteria were then grown at

419 25 ℃ overnight. Synchronized L1 larvae were placed on the plates at 20 ℃ until they reached
420 maturity. Young adult worms were used for further experiments.
421
422 **Construction of transgenic strains.** The vector expressing *lys-8p::gfp* was generated by
423 subcloning a 2011bp promoter fragment of *lys-8* into an expression vector (pPD95.75). The
424 vector was injected into the syncytial gonads of WT worms with 50 ng/ml pRF4 as a
425 transformation marker (Mello & Fire 1995). The transgenic worms carrying were confirmed
426 before assay.
427
428 **DAF-16 nuclear localization assay.** For the effect of aging on DAF‐16::GFP localization,
429 worms expressing *daf-16p::daf-16::gfp* were cultured on standard NGM plates at 20 ℃ for 1,
430 4, and 7 days, respectively. For indole treatment, young adults were transferred to NGM
431 plates containing 50-200 μM indole (Macklin, Shanghai, China) dissolved in DMSO for 24 h
432 at 20 ℃. NGM plates with equal amount of ethanol served as the control. After taken from
433 incubation, worms were immediately mounted in M9 onto microscope slides. The slides were
434 viewed using a Zeiss Axioskop 2 plus fluorescence microscope (Carl Zeiss, Jena, Germany)
435 with a digit camera. The status of DAF-16 localization was categorized as cytosolic
436 localization, nuclear localization when localization is observed throughout the entire body, or
437 intermediate localization when nuclear localization is visible, but not completely throughout
438 the body (Oh *et al.* 2005). At least 35 nematodes were counted in each experiment.
439
440 **Fluorescence microscopic analysis.** For imaging fluorescence, worms expressing

441 *hsp-16.2p::nCherry*, *dod-3p::gfp*, *lys-7p::gfp*, and *lys-8p::gfp* were mounted in M9 onto
442 microscope slides. The slides were imaged using a Zeiss Axioskop 2 Plus fluorescence
443 microscope. The intensities of nCherry and GFP were analyzed using the ImageJ software
444 (NIH). Three plates of at least 35 animals per plate were tested per assay, and all experiments
445 were performed three times independently.
446
447 **Lifespan analysis.** Synchronized L1 larvae were grown on NGM agar plates seeded with *E.*
448 *coli* OP50 at 20 ℃ until they reached the young adult stage. All the lifespan assays started
449 from the young adult stage at 20 ° C. The first day of adulthood was recorded as Day 1.
450 From Day 1 to Day 10, the worms were transferred to new NGM plates containing *E. coli*
451 strains at 20 °C daily. After that, worms were transferred every third day. The number of
452 worms was counted every day. Worms that did not move when gently prodded and displayed
453 no pharyngeal pumping were marked as dead.
454
455 **Age-related phenotypic marker assays.** The following two age-related phenotypes were
456 scored in 1- and 7-day-old worms (Chen *et al.* 2019). Pharyngeal pumping was measured by
457 counting the number of contractions in the terminal bulb of pharynx in 30 s intervals. Body
458 bending was measured by counting the number of body bends in 30 s intervals. At least 20
459 animals were determined per assay in 5 independent experiments.
460
461 **Intestinal barrier function assay in worms.** Intestinal barrier function was determined
462 according to the method described previously (Ma *et al.* 2020). Briefly, synchronized young

463 adult animals were cultured on standard NGM plates at 20 ℃ for 1, 4, 7, and 10 days. After
464 removed from the NGM plates, these animals were suspended in M9 liquid medium
465 containing *E. coli* OP50 (OD = 0.5-0.6), 5 % food dye FD&C Blue No. 1 (Bis[4-(N-ethyl-
466 N-3-sulfophenylmethyl) aminophenyl]-2-sulfophenylmethylium disodium salt)
467 (AccuStandard, New Haven, CT), and incubated for 6 h. After collected and washed with M9
468 buffer four times, the worms were mounted in M9 onto microscope slides. The slides were
469 viewed using a Zeiss Axioskop 2 Plus fluorescence microscope (Carl Zeiss, Jena, Germany)
470 to measure the leakage of the dyes in the body cavity of animals. The rate of body-cavity
471 leakage was calculated as a percentage by dividing the number of animals with dye leakage
472 by the number of total animals. For each time point, five independent experiments were
473 carried out. In each experiment, at least 20 of worms were calculated.
474
475 **Detection of bacterial accumulation in worms.** For detection of *E. coli* accumulation,
476 worms were grown on NGM plates with *E. coli* expressing mCherry (The plasmids of
477 PMF440 purchased from addgene) for 1, 4, 7 days at 20 ℃. Then animals were collected and
478 soaked in M9 buffer containing 25 mM levamisole hydrochloride (Sangon Biotech Co.), 50
479 μg/ml kanamycin (Sangon Biotech Co.), and 100 μg/ml ampicillin (Sangon Biotech Co.) for
480 30 minutes at room temperature. Then worms were washed three times with M9 buffer. Some
481 of animals were mounted in M9 onto microscope slides. The slides were viewed using a Zeiss
482 Axioskop 2 plus fluorescence microscope (Carl Zeiss, Jena, Germany) with a digital camera.
483 At least 35 worms were examined per assay in three independent experiments. Meanwhile, at
484 least 30 of nematodes were transferred into 50 μl PBS plus 0.1 % Triton and ground. The

lysates were diluted by 10-fold serial dilutions in sterilized water and spread over LB agar plates with 100 μg/ml ampicillin. After incubation overnight at 37 ℃, the *E. coli* CFU was counted. For each group, 3-5 independent experiments were carried out.

**Isolation and identification of the active compound.** Ten liters of the *E. coli* OP50 culture supernatants were collected by centrifugation, and freeze-dried in a VirTis freeze dryer. The powders were then dissolved with 10 ml of methanol. The crude extract was loaded on to an Ultimate 3000 HPLC (Thermofisher, Waltham, MA) coupled with automated fraction collector in batches through a continuous gradient on an Agilent ZORBAX SB-C18 column (Agilent, 5 μm, 4.6 × 250 mm) at a column temperature of 40 ℃ to yield 45 fractions based on retention time and one fraction was collected per minute. The total flow rate was 1 ml/min; mobile phase A was 0.1 % formic acid in water; and mobile phase B was 0.1 % formic acid in acetonitrile. The HPLC conditions were manually optimized on the basis of separation patterns with the following gradient: 0-2 min, 10 % B; 10 min, 25 % B; 30 min, 35 % B; 35 min, 90 % B; 36 min, 95 % B; 40 min, 90 % B; 40.1 min, 10 % B; and 45 min, 10 % B. UV spectra were recorded at 204-400 nm. The injection volume for the extracts was 50 μl. These fractions were tested for detection of nuclear translocation of DAF-16::GFP in worms. We found that the 26th fraction, which was collected at 26-27 min, could induce nuclear translocation of DAF-16 in worms. The active fraction was further then purified by Sephadex LH-20 with methanol and a single candidate active compound was obtained. The purified compound was structurally elucidated with NMR and MS data. NMR experiments were carried out on a Bruker DRX-500 spectrometer (Bruker Corp., Madison, WI) with solvent as

internal standard. High-resolution ESI-MS data was performed on Q Exactive Focus UPLC - MS (Thermofisher) with a PDA detector and an Obitrap mass detector using positive mode electrospray ionization.

**Quantitative analysis of indole in worms.** For quantitation of indole in *C. elegans*, worms were collected, washed 3-5 times with M9 buffer, and lyophilized for 4-6 h using a VirTis freeze dryer. Dried pellets were weighed, and transferred to a 1.5 ml centrifuge tube. After grinded for 10 minutes in a tissue grinder, the samples were dissolved in 300 µl solvent (methanol: water 20: 80 % (v/v)). The mixtures were then grinded for another 10 minutes, and centrifuged at 12000×g for 5 min. The supernatants were collected, and filtered through 0.22 µm membranes for further analysis using LC-MS. LC-MS analyses were performed on a Q Exactive Focus UPLC-MS (Thermofisher) with an atmospheric pressure chemical ionization (APCI) source and operated with positive mode and coupled with Atlabtis dC18 column (Waters, 3µm, 2.1×150 mm). Five microliters of samples were injected to the LC-MS system for analysis. The total flow rate was 0.3 ml/min; mobile phase A was 0.1 % formic acid in water; and mobile phase B was 0.1 % formic acid in acetonitrile. A/B gradient started at 5 % B for 3 min after injection and increased linearly to 95 % B at 13 min, then back to 5 % B over 0.1 min and finally held at 5 % B for an additional 1.9 min to re-equilibrate the column. Quantitation of indole was then achieved using standard curves generated using indole standard. Standard curve concentrations at 10, 50, 100, 300, 500, 700 and 9000 pmol/L in the solvent (methanol: water 20: 80 %

(v/v)). The data were analyzed and processed using Xcalibur software (Thermofisher).

**Quantitative real-time RT-PCR analysis.** Total RNA from worms was isolated using Trizol reagent (Invitrogen, Carlsbad, CA). Random-primed cDNAs were generated by reverse transcription of the total RNA samples using a standard protocol. A quantitative real-time-PCR analysis was performed with a Roche Light Cycler 480 System (Roche Applied Science, Penzberg, Germany) using SYBR Premix (Takara, Dalian, China). The relative amount of *lys-7* or *lys-8* mRNA to *act-1* mRNA (an internal control) was calculated using the method described previously (Pfaffl 2001). The primers used for PCR were as follows: *act-1*: 5'- CGT GTT CCC ATC CAT TGT CG -3' (F), 5'- AAG GTG TGA TGC CAG ATC TTC -3' (R); *lys-7*: 5'- GTC TCC AGA GCC AGA CAA TCC -3' (F), 5'- CCA GTG ACT CCA CCG CTG TA -3' (R); *lys-8*: 5'- GCT TCA GTC TCC GTC AAG GTC -3'(F), 5'- TGA AGC TGG CTC AAT GAA AC -3' (R).

## Statistics

Differences in survival rates were analyzed using the log-rank test. Differences in mRNA levels, the percentage of body cavity-leakage, fluorescence intensity, and CFU were assessed by performing the unpaired t-test. Differences in DAF-16::GFP nuclear accumulation were analyzed using the two-way ANOVA. Differences in survival rates were analyzed using the log-rank test. Data were analyzed using GraphPad Prism 8.0.

## References

551 Agus A, Planchais J , Sokol H (2018). Gut Microbiota Regulation of Tryptophan
552 Metabolism in Health and Disease. *Cell host & microbe*. **23**, 716-724.
553 Alexeev EE, Lanis JM, Kao DJ, Campbell EL, Kelly CJ, Battista KD, Gerich ME, Jenkins BR,
554 Walk ST, Kominsky DJ , Colgan SP (2018). Microbiota-Derived Indole Metabolites
555 Promote Human and Murine Intestinal Homeostasis through Regulation of
556 Interleukin-10 Receptor. *The American journal of pathology*. **188**, 1183-1194.
557 Baba T, Ara T, Hasegawa M, Takai Y, Okumura Y, Baba M, Datsenko KA, Tomita M, Wanner
558 BL , Mori H (2006). Construction of Escherichia coli K-12 in-frame, single-gene
559 knockout mutants: the Keio collection. *Molecular systems biology*. **2**, 2006 0008.
560 Bana B , Cabreiro F (2019). The Microbiome and Aging. *Annual review of genetics*. **53**,
561 239-261.
562 Bansal T, Alaniz RC, Wood TK , Jayaraman A (2010). The bacterial signal indole increases
563 epithelial-cell tight-junction resistance and attenuates indicators of inflammation.
564 *Proceedings of the National Academy of Sciences of the United States of America*.
565 **107**, 228-233.
566 Becker T, Loch G, Beyer M, Zinke I, Aschenbrenner AC, Carrera P, Inhester T, Schultze JL ,
567 Hoch M (2010). FOXO-dependent regulation of innate immune homeostasis. *Nature*.
568 **463**, 369-373.
569 Berg M, Monnin D, Cho J, Nelson L, Crits-Christoph A , Shapira M (2019). TGFbeta/BMP
570 immune signaling affects abundance and function of C. elegans gut commensals.
571 *Nature communications*. **10**, 604.
572 Boehnisch C, Wong D, Habig M, Isermann K, Michiels NK, Roeder T, May RC ,

573 Schulenburg H (2011). Protist-type lysozymes of the nematode Caenorhabditis
574 elegans contribute to resistance against pathogenic Bacillus thuringiensis. *PloS one*. **6**,
575 e24619.
576 Cabreiro F , Gems D (2013). Worms need microbes too: microbiota, health and aging in
577 Caenorhabditis elegans. *EMBO molecular medicine*. **5**, 1300-1310.
578 Chant EL , Summers DK (2007). Indole signalling contributes to the stable maintenance of
579 Escherichia coli multicopy plasmids. *Molecular microbiology*. **63**, 35-43.
580 Chaudhuri J, Bose N, Gong J, Hall D, Rifkind A, Bhaumik D, Peiris TH, Chamoli M, Le CH,
581 Liu J, Lithgow GJ, Ramanathan A, Xu XZS , Kapahi P (2016). A Caenorhabditis
582 elegans Model Elucidates a Conserved Role for TRPA1-Nrf Signaling in Reactive
583 alpha-Dicarbonyl Detoxification. *Current biology : CB*. **26**, 3014-3025.
584 Chen YL, Tao J, Zhao PJ, Tang W, Xu JP, Zhang KQ , Zou CG (2019). Adiponectin receptor
585 PAQR-2 signaling senses low temperature to promote C. elegans longevity by
586 regulating autophagy. *Nature communications*. **10**, 2602.
587 Chimerel C, Field CM, Pinero-Fernandez S, Keyser UF , Summers DK (2012). Indole
588 prevents Escherichia coli cell division by modulating membrane potential.
589 *Biochimica et biophysica acta*. **1818**, 1590-1594.
590 De Arras L, Laws R, Leach SM, Pontis K, Freedman JH, Schwartz DA , Alper S (2014).
591 Comparative genomics RNAi screen identifies Eftud2 as a novel regulator of innate
592 immunity. *Genetics*. **197**, 485-496.
593 Dierking K, Yang W , Schulenburg H (2016). Antimicrobial effectors in the nematode
594 Caenorhabditis elegans: an outgroup to the Arthropoda. *Philosophical transactions of*

595 *the Royal Society of London. Series B, Biological sciences*. **371**.

596 Ezcurra M (2018). Dissecting cause and effect in host-microbiome interactions using the
597 combined worm-bug model system. *Biogerontology*. **19**, 567-578.

598 Garigan D, Hsu AL, Fraser AG, Kamath RS, Ahringer J , Kenyon C (2002). Genetic
599 analysis of tissue aging in Caenorhabditis elegans: a role for heat-shock factor and
600 bacterial proliferation. *Genetics*. **161**, 1101-1112.

601 Garsin DA, Villanueva JM, Begun J, Kim DH, Sifri CD, Calderwood SB, Ruvkun G ,
602 Ausubel FM (2003). Long-lived C. elegans daf-2 mutants are resistant to bacterial
603 pathogens. *Science*. **300**, 1921.

604 Gupta A , Singh V (2017). GPCR Signaling in C. elegans and Its Implications in Immune
605 Response. *Advances in immunology*. **136**, 203-226.

606 Honda K , Littman DR (2012). The microbiome in infectious disease and inflammation.
607 *Annual review of immunology*. **30**, 759-795.

608 Hwang AB, Ryu EA, Artan M, Chang HW, Kabir MH, Nam HJ, Lee D, Yang JS, Kim S, Mair
609 WB, Lee C, Lee SS , Lee SJ (2014). Feedback regulation via AMPK and HIF-1
610 mediates ROS-dependent longevity in Caenorhabditis elegans. *Proceedings of the*
611 *National Academy of Sciences of the United States of America*. **111**, E4458-4467.

612 Irazoqui JE, Troemel ER, Feinbaum RL, Luhachack LG, Cezairliyan BO , Ausubel FM
613 (2010a). Distinct pathogenesis and host responses during infection of C. elegans by P.
614 aeruginosa and S. aureus. *PLoS pathogens*. **6**, e1000982.

615 Irazoqui JE, Urbach JM , Ausubel FM (2010b). Evolution of host innate defence: insights
616 from Caenorhabditis elegans and primitive invertebrates. *Nature reviews.*

*Immunology*. **10**, 47-58.

Johnson KV , Foster KR (2018). Why does the microbiome affect behaviour? *Nature reviews. Microbiology*. **16**, 647-655.

Kamath RS , Ahringer J (2003). Genome-wide RNAi screening in Caenorhabditis elegans. *Methods*. **30**, 313-321.

Kim DH, Feinbaum R, Alloing G, Emerson FE, Garsin DA, Inoue H, Tanaka-Hino M, Hisamoto N, Matsumoto K, Tan MW , Ausubel FM (2002). A conserved p38 MAP kinase pathway in Caenorhabditis elegans innate immunity. *Science*. **297**, 623-626.

Kindt KS, Viswanath V, Macpherson L, Quast K, Hu H, Patapoutian A , Schafer WR (2007). Caenorhabditis elegans TRPA-1 functions in mechanosensation. *Nature neuroscience*. **10**, 568-577.

Lee JH, Wood TK , Lee J (2015). Roles of indole as an interspecies and interkingdom signaling molecule. *Trends in microbiology*. **23**, 707-718.

Lee WJ , Brey PT (2013). How microbiomes influence metazoan development: insights from history and Drosophila modeling of gut-microbe interactions. *Annual review of cell and developmental biology*. **29**, 571-592.

Li ST, Zhao HQ, Zhang P, Liang CY, Zhang YP, Hsu AL , Dong MQ (2019). DAF-16 stabilizes the aging transcriptome and is activated in mid-aged Caenorhabditis elegans to cope with internal stress. *Aging cell*. **18**, e12896.

Ma YC, Yang ZS, Ma LQ, Shu R, Zou CG , Zhang KQ (2020). YAP in epithelium senses gut barrier loss to deploy defenses against pathogens. *PLoS pathogens*. **16**, e1008766.

Mallo GV, Kurz CL, Couillault C, Pujol N, Granjeaud S, Kohara Y , Ewbank JJ (2002).

639 Inducible antibacterial defense system in C. elegans. *Current biology : CB*. **12**,
640 1209-1214.
641 Manichanh C, Borruel N, Casellas F , Guarner F (2012). The gut microbiota in IBD. *Nature*
642 *reviews. Gastroenterology & hepatology*. **9**, 599-608.
643 Marsh EK, van den Berg MC , May RC (2011). A two-gene balance regulates Salmonella
644 typhimurium tolerance in the nematode Caenorhabditis elegans. *PloS one*. **6**, e16839.
645 McGee MD, Weber D, Day N, Vitelli C, Crippen D, Herndon LA, Hall DH , Melov S
646 (2011). Loss of intestinal nuclei and intestinal integrity in aging C. elegans. *Aging cell*.
647 **10**, 699-710.
648 Mello C , Fire A (1995). DNA transformation. *Methods in cell biology*. **48**, 451-482.
649 Montalvo-Katz S, Huang H, Appel MD, Berg M , Shapira M (2013). Association with soil
650 bacteria enhances p38-dependent infection resistance in Caenorhabditis elegans.
651 *Infection and immunity*. **81**, 514-520.
652 Nandakumar M , Tan MW (2008). Gamma-linolenic and stearidonic acids are required for
653 basal immunity in Caenorhabditis elegans through their effects on p38 MAP kinase
654 activity. *PLoS genetics*. **4**, e1000273.
655 O'Donnell MP, Fox BW, Chao PH, Schroeder FC , Sengupta P (2020). A neurotransmitter
656 produced by gut bacteria modulates host sensory behaviour. *Nature*. **583**, 415-420.
657 O'Rourke D, Baban D, Demidova M, Mott R , Hodgkin J (2006). Genomic clusters, putative
658 pathogen recognition molecules, and antimicrobial genes are induced by infection of
659 C. elegans with M. nematophilum. *Genome research*. **16**, 1005-1016.
660 Oh S, Go GW, Mylonakis E , Kim Y (2012). The bacterial signalling molecule indole

attenuates the virulence of the fungal pathogen Candida albicans. *Journal of applied microbiology*. **113**, 622-628.

Oh SW, Mukhopadhyay A, Svrzikapa N, Jiang F, Davis RJ , Tissenbaum HA (2005). JNK regulates lifespan in Caenorhabditis elegans by modulating nuclear translocation of forkhead transcription factor/DAF-16. *Proceedings of the National Academy of Sciences of the United States of America*. **102**, 4494-4499.

Pfaffl MW (2001). A new mathematical model for relative quantification in real-time RT-PCR. *Nucleic acids research*. **29**, e45.

Portal-Celhay C , Blaser MJ (2012). Competition and resilience between founder and introduced bacteria in the Caenorhabditis elegans gut. *Infection and immunity*. **80**, 1288-1299.

Portal-Celhay C, Bradley ER , Blaser MJ (2012). Control of intestinal bacterial proliferation in regulation of lifespan in Caenorhabditis elegans. *BMC microbiology*. **12**, 49.

Simonsen KT, Moller-Jensen J, Kristensen AR, Andersen JS, Riddle DL , Kallipolitis BH (2011). Quantitative proteomics identifies ferritin in the innate immune response of C. elegans. *Virulence*. **2**, 120-130.

Singh V , Aballay A (2006). Heat-shock transcription factor (HSF)-1 pathway required for Caenorhabditis elegans immunity. *Proceedings of the National Academy of Sciences of the United States of America*. **103**, 13092-13097.

Sommer F , Backhed F (2013). The gut microbiota--masters of host development and physiology. *Nature reviews. Microbiology*. **11**, 227-238.

Sonowal R, Swimm A, Sahoo A, Luo L, Matsunaga Y, Wu Z, Bhingarde JA, Ejzak EA,

683 Ranawade A, Qadota H, Powell DN, Capaldo CT, Flacker JM, Jones RM, Benian
684 GM , Kalman D (2017). Indoles from commensal bacteria extend healthspan.
685 *Proceedings of the National Academy of Sciences of the United States of America*.
686 **114**, E7506-E7515.
687 Tan MW , Shapira M (2011). Genetic and molecular analysis of nematode-microbe
688 interactions. *Cellular microbiology*. **13**, 497-507.
689 Venkatachalam K , Montell C (2007). TRP channels. *Annual review of biochemistry*. **76**,
690 387-417.
691 Visvikis O, Ihuegbu N, Labed SA, Luhachack LG, Alves AF, Wollenberg AC, Stuart LM,
692 Stormo GD , Irazoqui JE (2014). Innate host defense requires TFEB-mediated
693 transcription of cytoprotective and antimicrobial genes. *Immunity*. **40**, 896-909.
694 Wu H, Tremaroli V , Backhed F (2015). Linking Microbiota to Human Diseases: A Systems
695 Biology Perspective. *Trends in endocrinology and metabolism: TEM*. **26**, 758-770.
696 Xiao R, Zhang B, Dong Y, Gong J, Xu T, Liu J , Xu XZ (2013). A genetic program
697 promotes C. elegans longevity at cold temperatures via a thermosensitive TRP
698 channel. *Cell*. **152**, 806-817.
699 Ye L, Bae M, Cassilly CD, Jabba SV, Thorpe DW, Martin AM, Lu HY, Wang J, Thompson JD,
700 Lickwar CR, Poss KD, Keating DJ, Jordt SE, Clardy J, Liddle RA , Rawls JF
701 (2021). Enteroendocrine cells sense bacterial tryptophan catabolites to activate enteric
702 and vagal neuronal pathways. *Cell host & microbe*. **29**, 179-196 e179.
703 Zarkan A, Liu J, Matuszewska M, Gaimster H , Summers DK (2020). Local and Universal
704 Action: The Paradoxes of Indole Signalling in Bacteria. *Trends in microbiology*. **28**,

566-577.

Zhang J, Holdorf AD , Walhout AJ (2017). C. elegans and its bacterial diet as a model for systems-level understanding of host-microbiota interactions. *Current opinion in biotechnology*. **46**, 74-80.

Zou CG, Tu Q, Niu J, Ji XL , Zhang KQ (2013). The DAF-16/FOXO transcription factor functions as a regulator of epidermal innate immunity. *PLoS pathogens*. **9**, e1003660.

Zugasti O , Ewbank JJ (2009). Neuroimmune regulation of antimicrobial peptide expression by a noncanonical TGF-beta signaling pathway in Caenorhabditis elegans epidermis. *Nature immunology*. **10**, 249-256.

## Acknowledgments

We thank the Caenorhabditis Genetics Center, Dr. Gary Ruvkun, and Dr. Mengqiu Dong for nematode strains. This work was supported by a grant from the National Key R&D Program of China (2022YFD1400700), the National Natural Science Foundation of China (U1802233 and 31900420), and the independent research fund of Yunnan Characteristic Plant Extraction Laboratory (2022YKZY006).

## Author Contributions

C.G.Z., Y.C.M., and R.Q.Y. designed the experiments and analyzed the data. R.Q.Y., Y.H.C., Q.Y.W., J.T., S.Z.N., and Q.Z performed the experiments. C.G.Z., Y.C.M., R.Q.Y., and Y.H. C. interpreted the data. C.G.Z. and Y.C.M. wrote the manuscript.

727 **Competing interests:** The authors declare no competing interests.

728

729 **Data availability statement:** All data generated or analyzed during this study are included in

730 the manuscript and supporting source data file.

731

732

733

734

735

736

737

738

739

740

741

742

743

744

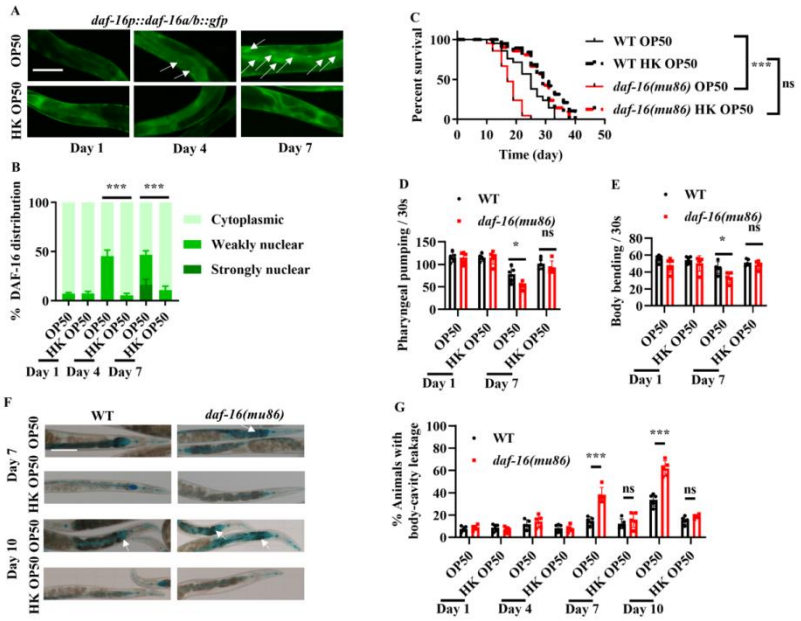


745

746 **Figure 1. Activation of DAF-16 by bacterial accumulation is required for maintenance of**

747 **longevity and organismal fitness.**

748 **(A)** The nuclear translocation of DAF-16::GFP in the intestine was increased in worms fed

749 live *E. coli* OP50, but not in worms fed heat-killed (HK) *E. coli* OP50. White arrows indicate

750 nuclear localization of DAF-16::GFP. Scale bars: 50 μm. **(B)** Quantification of DAF-16

751 nuclear localization. These results are means ± SEM of three independent experiments (n > 35

752 worms per experiment). ***$P$ < 0.001. $P$-values were calculated using the using the two-way

753 ANOVA. **(C)** *daf-16(mu86)* mutants grown on live *E. coli* OP50 had a shorter lifespan

754 compared to those grown on HK *E. coli* OP50. ***$P$ < 0.001. ns, not significant. $P$-values

755 were calculated using a Log-rank test. **(D and E)** DAF-16 is involved in delaying the

756 appearance of the aging markers, including pharyngeal pumping (D) and body bending (E), in

757 worms fed live *E. coli* OP50, but not in worms fed HK *E. coli* OP50. These results are means

758 ± SEM of five independent experiments (n > 20 worms per experiment). *$P$ < 0.05. ns, not

759 significant. (F) Representative images of intestinal permeability stained by food dye FD&C

760 Blue No. 1 in worms. White arrows indicate the body-cavity leakages of worms. Scale bars:
761 100 μm. **(G)** Quantification of body-cavity leakages was measured in animals fed on live *E.*
762 *coli* OP50 or heat-killed (HK) *E. coli* OP50 over time. These results are means ± SEM of five
763 independent experiments (n > 20 worms per experiment). ***$P < 0.001$. ns, not significant.
764 *P*-values (**D, E, and G**) were calculated using the unpaired t-test.

765 **Figure 1-source data 1**

766 **Lifespan assays summary and quantification results.**

767

768

769

770

771

772

773

774

775

776

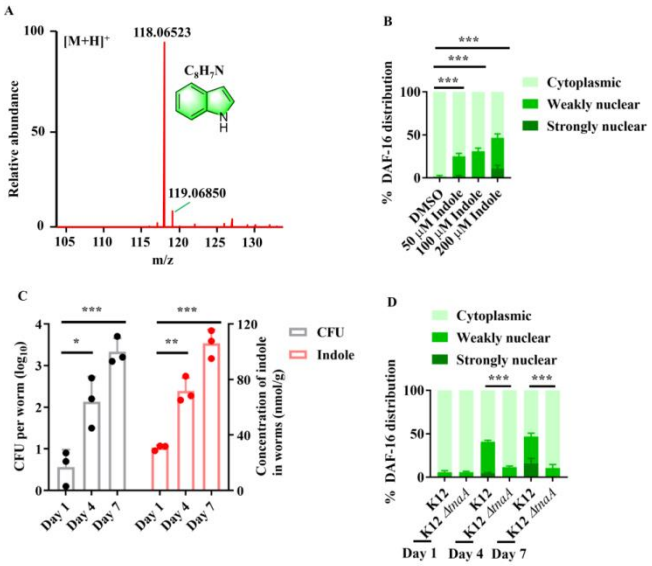


**Figure 2. Indole is involved in the nuclear translocation of DAF-16 in worms with age.**

**(A)** High-resolution mass spectrum of indole. The corresponding 1H and13C NMR spectra were depicted in Figure 2-figure supplement 1 and Table S1. **(B)** Supplementation with indole promoted nuclear translocation of DAF-16::GFP in the intestine of worms. These results are means ± SEM of three independent experiments (n > 35 worms per experiment). ***$P$ < 0.001. **(C)** Colony-forming units (CFU) of *E. coli* OP50 were increased in worms over time, which was accompanied by an increase in the levels of indole in worms. These results are means ± SEM of three independent experiments (n > 30 worms per experiment). *$P$ < 0.05; **$P$ < 0.01; ***$P$ < 0.001. $P$-values **(C)** were calculated using the unpaired t-test. **(D)** Deletion of *tnaA* significantly suppressed the nuclear translocation of DAF-16::GFP in the intestine of worms fed *E. coli* BW25113. These results are means ± SEM of three independent experiments (n > 35 worms per experiment). ***$P$ < 0.001. $P$-values (**B and D**) were calculated using the two-way ANOVA.

**Figure 2-source data 1**

**Quantification results.**

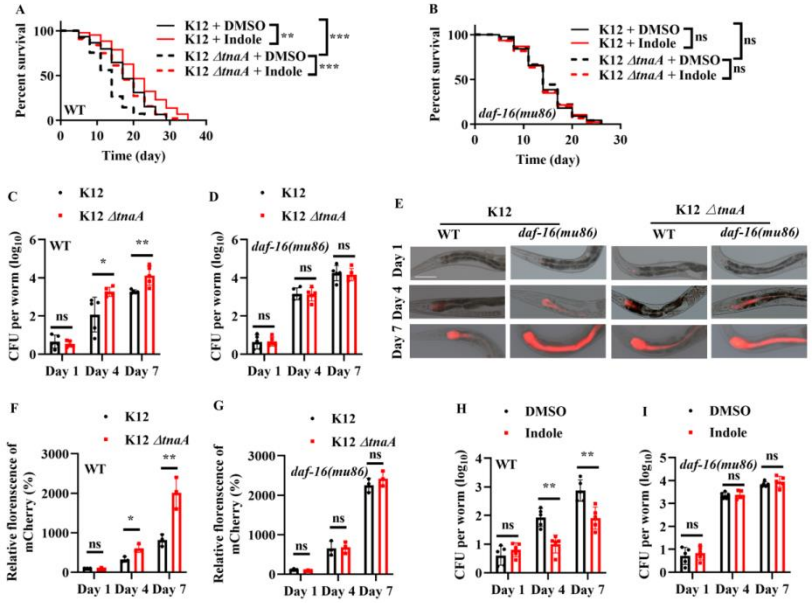


**Figure 3. Indole is required for maintenance of normal lifespan via DAF-16 in worms.**

**(A)** Wild type (WT) worms fed *E. coli* K-12 *ΔtnaA* strains had a shorter lifespan compared to those fed *E. coli* K-12 strain at 20 °C. Supplementation with indole (100 μM) extended lifespan of WT worms fed *E. coli* K-12, and rescued the short lifespan of WT worms fed *E. coli* K-12 *ΔtnaA* strain. ***P* < 0.01. ****P* < 0.001. **(B)** Indole-mediated lifespan extension depended on DAF-16 in worms. ns, not significant. *P*-values (**A and B)** were calculated using log-rank test. **(C and D)** Colony-forming units (CFU) of *E. coli K-12* or K-12 *ΔtnaA* were measured in WT worms (C) or *daf-16(mu86)* mutants (D). These results are means ± SEM of five independent experiments (n > 30 worms per experiment). **P* < 0.05; ***P* < 0.01. ns, not significant. **(E)** Fluorescence images of worms exposed to *E. coli* K-12 or K-12 *ΔtnaA* expressing mCherry. Scale bars: 50 μm. (**F and G**) Quantification of fluorescent intensity of *E. coli* K-12 or K-12 *ΔtnaA* expressing mCherry in WT worms (F) or *daf-16(mu86)* mutants (G). These results are means ± SEM of three independent experiments (n > 35 worms per experiment). **P* < 0.05. ***P* < 0.01. ns, not significant. **(H and I)** CFU of *E. coli* K-12 were

808 measured in WT worms (H) or *daf-16(mu86)* mutants (I) in the presence of exogenous with
809 indole (100 μM). These results are means ± SEM of five independent experiments (n > 30
810 worms per experiment). ***P* < 0.01. ns, not significant. *P*-values (**C, D, and F-I**) were
811 calculated using the unpaired t-test.

812 **Figure 3-source data 1**

813 **Lifespan assays summary and quantification results.**

814

815

816

817

818

819

820

821

822

823

824

825

826

827

828

829

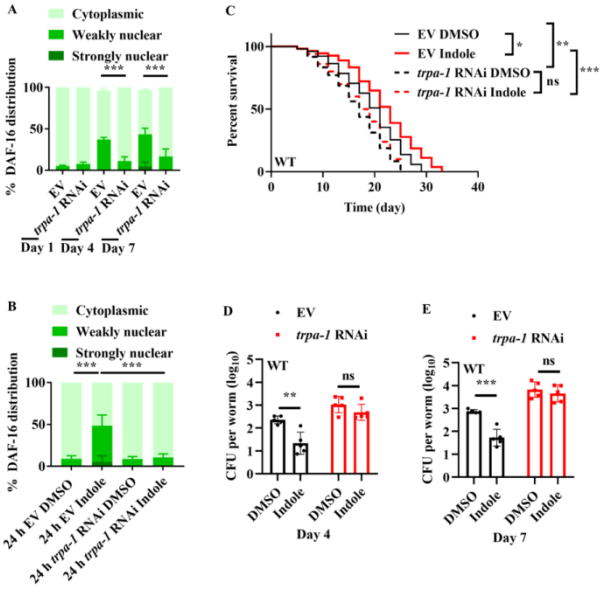


**Figure 4. TRPA-1 is involved in indole-mediated DAF-16 activation.**

**(A and B)** Knockdown of *trpa-1* by RNAi suppressed nuclear translocation of DAF-16::GFP in worms on Days 4 and 7 (A), or in young adult worms treated with indole (100 μM) for 24 h (B). EV, empty vector. These results are means ± SEM of three independent experiments (n > 35 worms per experiment). ***$P$ < 0.001. ns, not significant. $P$-values (**A and B**) were calculated using the two-way ANOVA. **(C)** Knockdown of *trpa-1* by RNAi significantly shortened the lifespan in worms treated with indole (100 μM). *$P$ < 0.05; **$P$ < 0.01; ***$P$ < 0.001. $P$-values were calculated using log-rank test. **(D and E)** Colony-forming units (CFU) of *E. coli* K12 were significantly increased in worms subjected to *trpa-1* RNAi on Days 4 (D) and 7 (E). Meanwhile, supplementation with indole (100 μM) failed to suppress the increases in CFU in *trpa-1* (RNAi) worms. These results are means ± SEM of five independent experiments (n > 30 worms per experiment). **$P$ < 0.01; ***$P$ < 0.001. ns, not significant. $P$-values (**D** and **E**) were calculated using the unpaired t-test.

**Figure 4-source data 1**

**Lifespan assays summary and quantification results.**

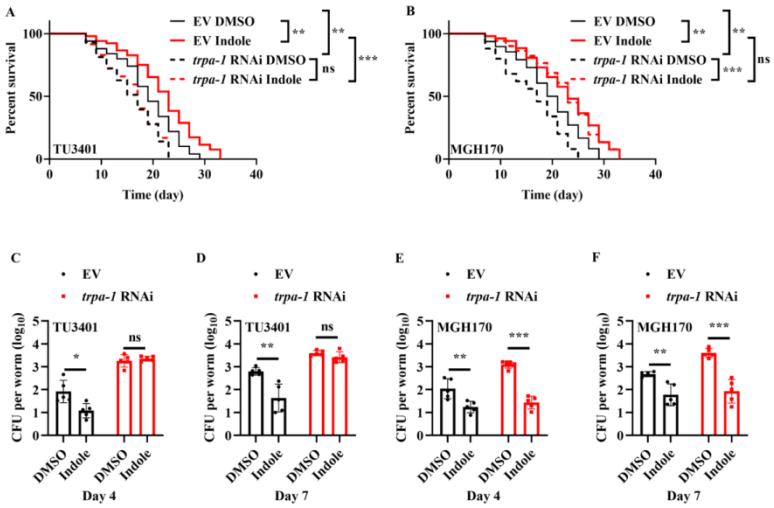


**Figure 5. TRPA-1 in neurons is involved in indole-mediated longevity.**

**(A and B)** Either neuronal - (A) or intestinal -(B) specific *trpa-1* RNAi shortened lifespan in worms. However, supplementation with indole (100 μM) significantly extended lifespan in worms after knockdown of *trpa-1* by RNAi in the intestine, but not in neurons. EV, empty vector. $^{**}P < 0.01$; $^{***}P < 0.001$. ns, not significant. *P*-values (**A** and **B**) were calculated using log-rank test. **(C and D)** Supplementation with indole (100 μM) no longer inhibited colony-forming units (CFU) of *E. coli* K12 in worms on Days 4 (C) and 7 (D) after knockdown of *trpa-1* by RNAi in neurons. These results are means ± SEM of five independent experiments (n > 30 worms per experiment). $^{*}P < 0.05$; $^{**}P < 0.01$. ns, not significant. **(E and F)** Supplementation with indole (100 μM) significantly suppressed the CFU of *E. coli* K-12 in worms subjected to intestinal-specific *trpa-1* RNAi on Days 4 (E) and 7 (F). These results are means ± SEM of five independent experiments (n > 30 worms per experiment). $^{**}P < 0.01$; $^{***}P < 0.001$. ns, not significant. *P*-values (**C**-**F**) were calculated using the unpaired t-test.

**Figure 5-source data 1**

**Lifespan assays summary and quantification results.**

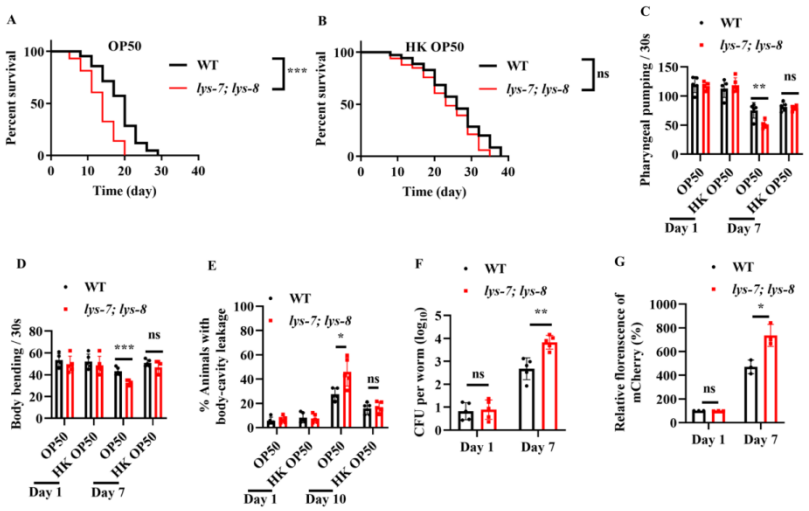


**Figure 6. LYS-7 and LYS-8 are required for maintenance of normal lifespan in worms.**

**(A and B)** The lifespans of worms fed either live *E. coli* OP50 (A) or fed heat-killed (HK) *E. coli* OP50 (B). The *lys-7(ok1384); lys-8(ok3504)* double mutants exhibited a shorter lifespan compared to wild-type (WT) worms fed live *E. coli* OP50 (A). By contrast, the lifespan in the *lys-7(ok1384); lys-8(ok3504)* double mutants was comparable of that in WT worms fed HK *E. coli* OP50 (B). ***$P < 0.001$. ns, not significant. *P*-values (**A** and **B**) were calculated using log-rank test. **(C-E)** *lys-7* and *lys-8* were involved in delaying the appearance of the aging markers, including pharyngeal pumping (C), body bending (D), and body-cavity leakage (E) in worms fed live *E. coli* OP50. These results are means ± SEM of five independent experiments (n > 20 worms per experiment). *$P < 0.05$; **$P < 0.01$; ***$P < 0.001$. **(F)** Colony-forming units (CFU) of *E. coli* OP50 were significantly increased in *lys-7(ok1384);lys-8(ok3504)* double mutants on Day 7. These results are means ± SEM of five independent experiments (n > 20 worms per experiment). **$P < 0.01$. ns, not significant. **(G)** Quantification of fluorescent intensity of *E. coli* OP50 expressing mCherry in *lys-7(ok1384);lys-8(ok3504)* double mutants. These results are means ± SEM of three independent experiments (n > 35 worms per experiment). *$P < 0.05$. ns, not significant.

*P*-values (**C-G**) were calculated using the unpaired t-test.

**Figure 6-source data 1**

**Lifespan assays summary and quantification results.**

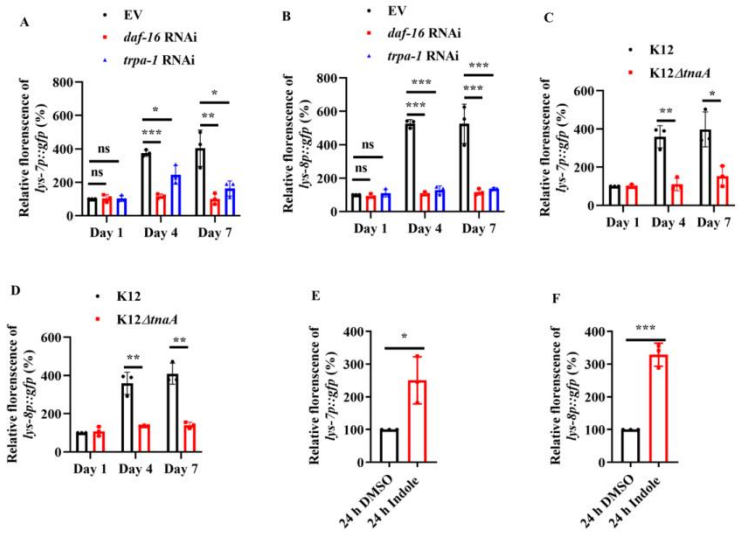


**Figure 7. The expressions of *lys-7* and *lys-8* were up-regulated by the indole/TRPA-1/DAF-16 signaling.**

**(A and B)** The expression of either *lys-7p::gfp* (A) or *lys-8p::gfp* (B) was significantly suppressed after knockdown of *daf-16* or *trpa-1* by RNAi in worms fed live *E. coli* OP50 on Days 4 and 7. EV, empty vector. **(C and D)** The expression of either *lys-7p::gfp* (C) or *lys-8p::gfp* (D) was reduced in worms fed *E. coli* K-12 *ΔtnaA* strain on Days 4 and 7, compared with that in age-matched worms fed *E. coli* K-12. **(E and F)** Indole (100 μM) remarkably increased the expression of either *lys-7p::gfp* (E) or *lys-8::gfp* (F) in young adult worms after 24 h of treatment. These results are means ± SEM of three independent experiments (n > 35 worms per experiment). **P* < 0.05. ***P* < 0.01. ****P* < 0.001. ns, not significant. *P*-values (**A-H**) were calculated using the unpaired t-test.

**Figure 7-source data 1**

**Quantification results.**

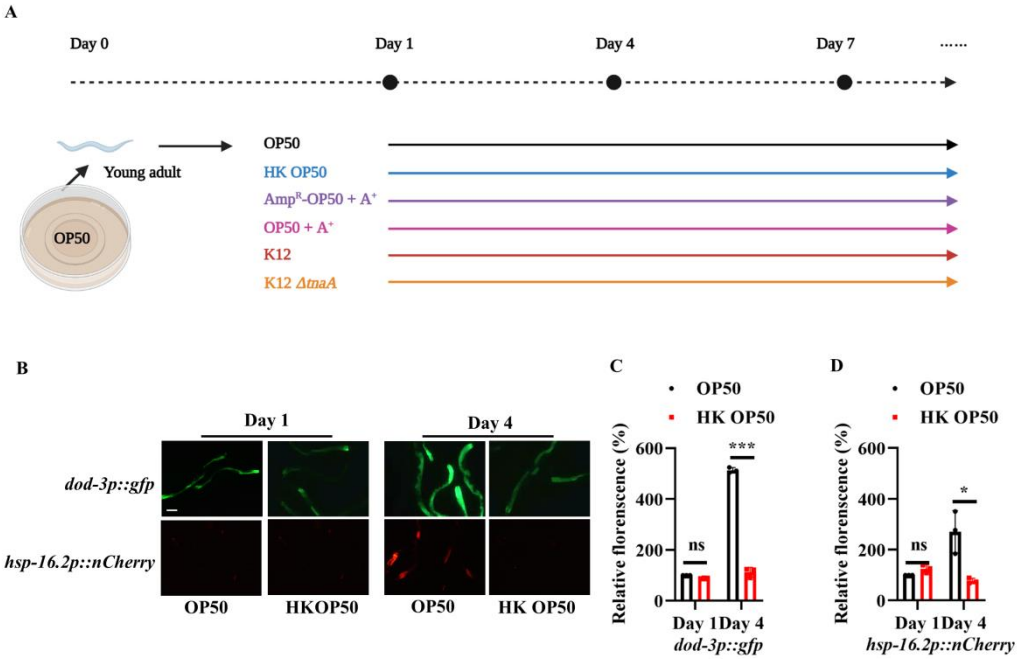


**Figure 1-figure supplement 1. The expression of two DAF-16 target genes *dod-3* and *hsp-16.2* is significantly up-regulated in worms fed live *E. coli* OP50 on Day 4.**

(**A**) Study design for age-related dysbiosis study. (**B**) Representative images of worms expressing *dod-3p::gfp* and *hsp-16.2p::nCherry* fed live or heat-killed (HK) *E. coli* OP50 on Days 1 and 4. Scale bars: 100 μm. (**C** and **D**) Quantification of fluorescent intensity of *dod-3p::gfp* (C), and *hsp-16.2p::nCherry* (D). These results are means ± SEM of three independent experiments (n > 30 worms per experiment). ***$P < 0.001$; *$P < 0.05$. ns, not significant. *P*-values (**C** and **D**) were calculated using the unpaired t-test.

**Figure 1-figure supplement 1-source data 1**

**Quantification results.**

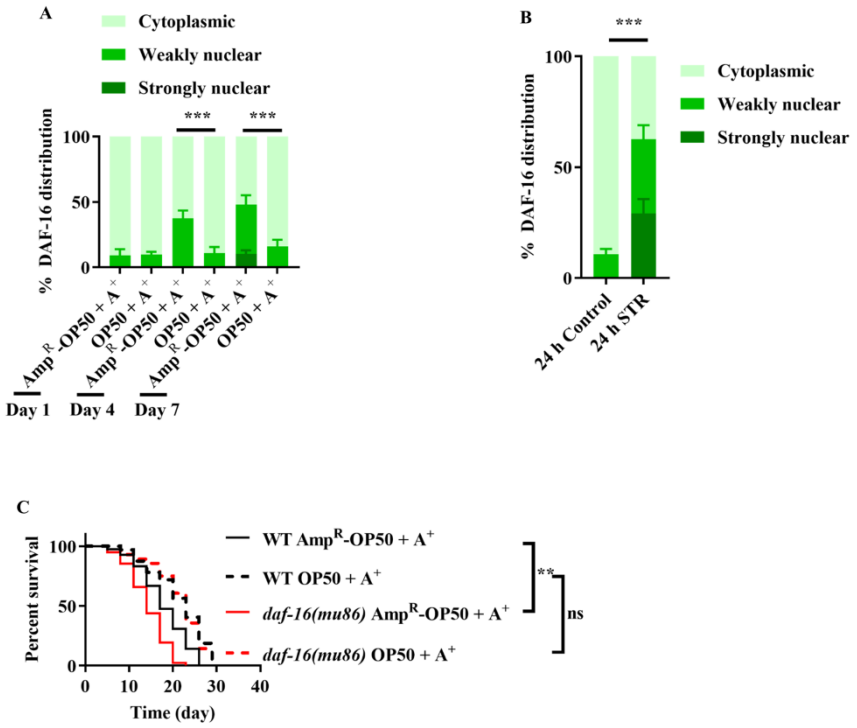


**Figure 1-figure- supplement 2. DAF -16 is not activated by antibiotic-killed *E. coli* OP50.**

(**A**) DAF-16 was also retained in the cytoplasm of the intestine of worms fed ampicillin-killed *E. coli* OP50 on Days 4 and 7. These results are means ± SEM of three independent experiments (n > 35 worms per experiment). ***$P$ < 0.001. (B) Starvation induced the nuclear translocation of DAF-16 in the intestine of worms on Day 1. These results are means ± SEM of three independent experiments (n > 35 worms per experiment). ***$P$ < 0.001. $P$-values (**A** and **B**) were calculated using two-way ANOVA. (**C**) *daf-16(mu86)* mutants grown on live *E. coli* OP50 had a shorter lifespan compared to those grown on ampicillin-killed *E. coli* OP50. **$P$ < 0.01. ns, not significant. $A^+$, Ampicillin treatment; $Amp^R$-OP50, *E. coli* OP50 containing an ampicillin resistance plasmid (PMF440). $P$-values throughout were calculated using log-rank test.

**Figure 1-figure supplement 2-source data 1**

**Lifespan assays summary and quantification results.**

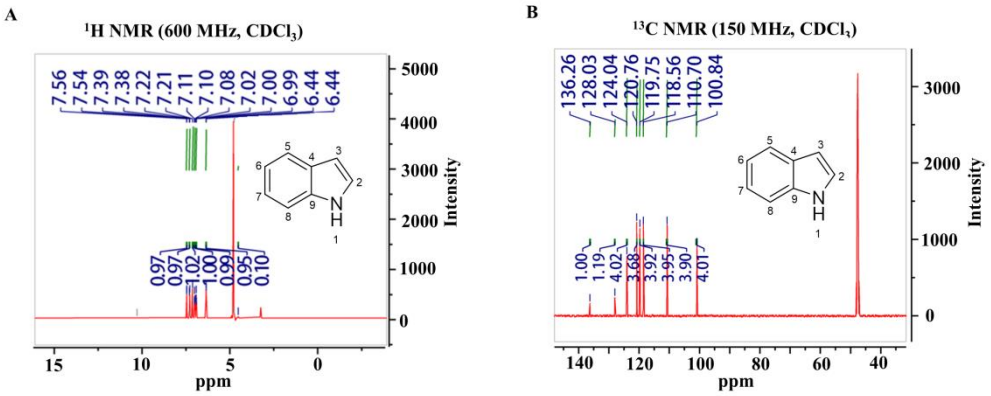


**Figure 2-figure supplement 1. Indole is the active compound for activation of DAF-16.**

**(A and B)** The candidate compound for activation of DAF-16 was identified as indole with $^{1}$H NMR (A) and $^{13}$C NMR (B).

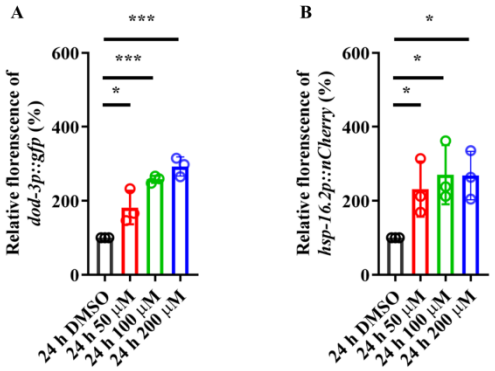


**Figure 2-figure supplement 2. Indole treatment induces the expressions of two DAF-16 target genes in worms**

**(A and B)** Quantification of fluorescent intensity of *dod-3p::gfp* (A) or *hsp-16.2p::nCherry* (B) in young adult worms treated with indole (100 μM). These results are means ± SEM of three independent experiments (n > 35 worms per experiment). **P* < 0.05; ****P* < 0.001. *P*-values throughout were calculated using the unpaired t-test.

**Figure 2-figure supplement 2-source data 1**

**Quantification results.**

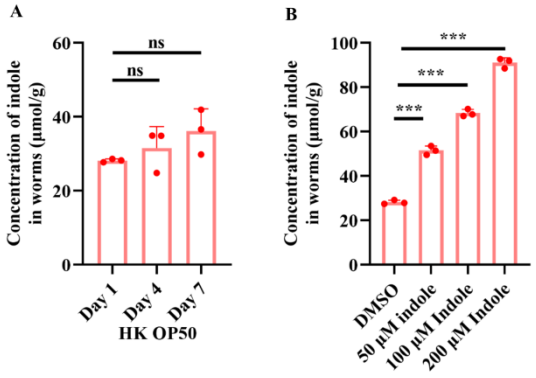


**Figure 2-figure supplement 3. Quantitative analysis of indole in *C. elegans* by LC-MS.**

(**A**) The levels of indole were not altered in worms fed heat-killed (HK) *E. coli* OP50 on Days 1, 4, and 7. These results are means ± SEM of three independent experiments. ns, not significant. (**B**) Supplementation with indole (50-200 μM) significantly increased the indole levels in young adult worms after 24 h treatment. These results are means ± SEM of three independent experiments. ***$P < 0.001$. *P*-values throughout were calculated using the unpaired t-test.

**Figure 2-figure supplement 3-source data 1**

**Quantification results.**

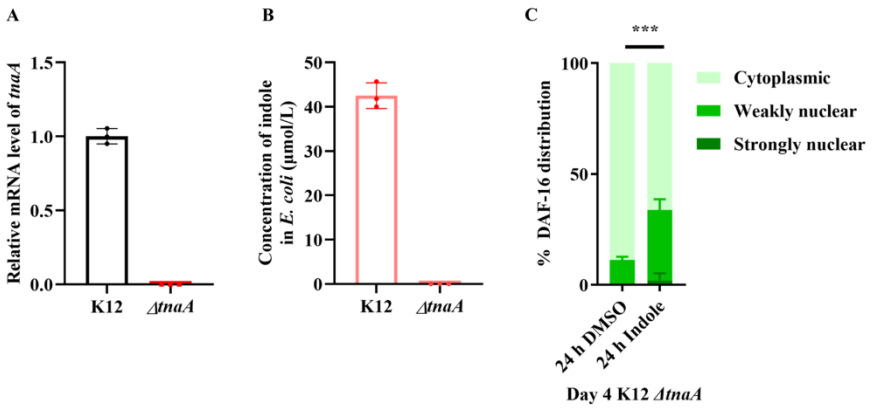


**Figure 2-figure supplement 4. Functional validation of *tnaA*-deficient BW25113 strain.**

(**A and B**) The levels of *tnaA* mRNA (A) and indole (B) were undetectable in the K-12 Δ*tnaA* strains. These results are means ± SEM of three independent experiments. (**C**) The nuclear translocation of DAF-16::GFP was mainly located in the cytoplasm of the intestine in worms fed live K-12 Δ*tnaA* strains on Day 4. However, supplementation with indole (100 μM) induced the nuclear translocation of DAF-16::GFP in the intestine in these worms. These results are means ± SEM of three independent experiments. $^{**}P < 0.01$. *P*-value was calculated using the Friedman test (with Dunn's test for multiple comparisons).

**Figure 2-figure supplement 4-source data 1**

**Quantification results.**

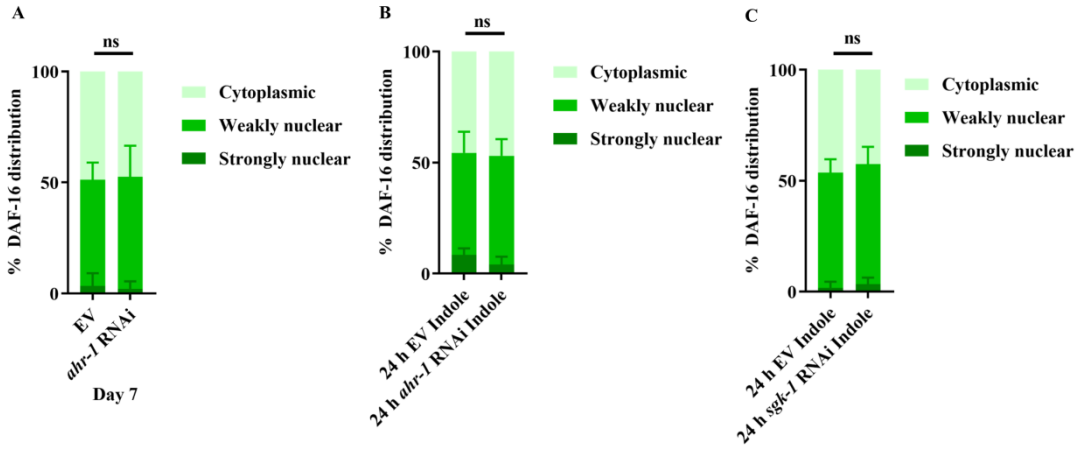


**Figure 4-figure supplement 1. Indole promotes nuclear localization of DAF-16 independent of AHR-1 and SGK-1.**

**(A and B)** Knockdown of *ahr-1* by RNAi did not affect the nuclear translocation of DAF-16 in worms fed K12 strain on Day 7 (A) or young adult worms treated with indole for 24 h (B). These results are means ± SEM of three independent experiments (n > 35 worms per experiment). **(C)** Knockdown of *sgk-1* by RNAi did not affect the nuclear translocation of DAF-16 in young adult worms treated with indole (100 μM) for 24 h. These results are means ± SEM of three independent experiments (n > 35 worms per experiment). ns, not significant. *P*-value throughout was calculated using two-way ANOVA.

**Figure 4-figure supplement 1-source data 1**

**Quantification results.**

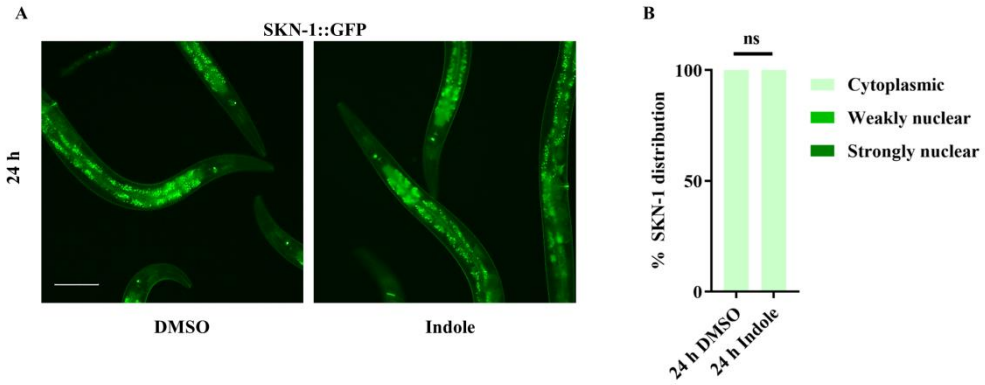


**Figure 4-figure supplement 2. Supplementation with indole fails to induce nuclear localization of SKN-1::GFP in worms.**

(**A**) Representative images of SKN-1::GFP. Scale bars: 100 μm. (**B**) Quantification of SKN-1 nuclear localization. These results are means ± SEM of three independent experiments (n > 35 worms per experiment). ns, not significant. *P*-value was calculated using the using the two-way ANOVA.

**Figure 4-figure supplement 2-source data 1**

**Quantification results.**

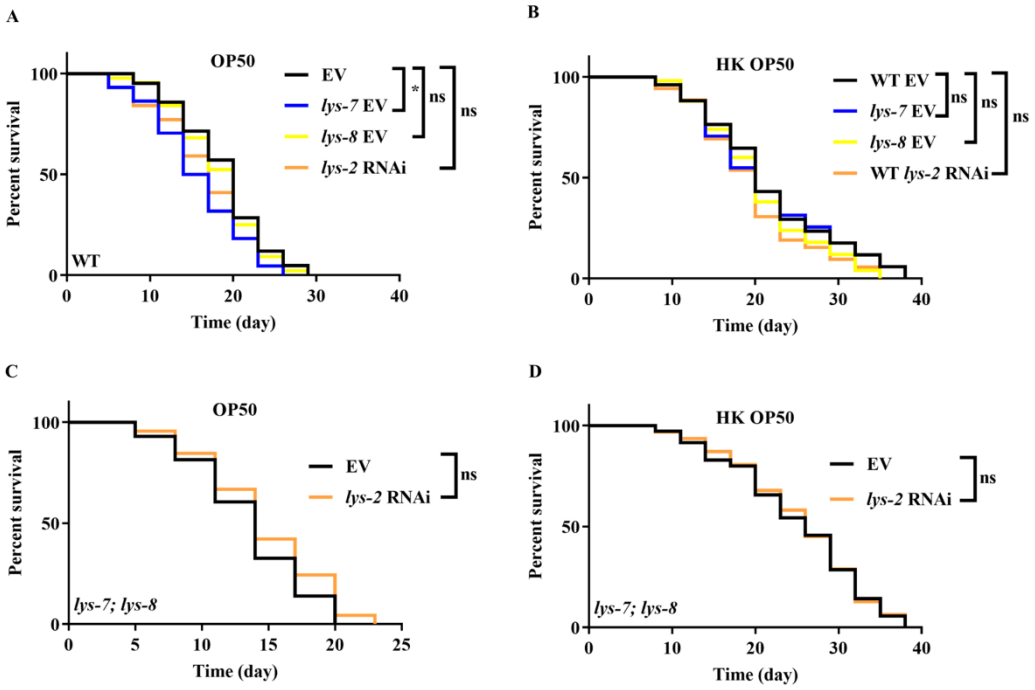


**Figure 6-figure supplement 1. The roles of lysozyme genes in lifespan in worms.**

**(A and B)** The lifespans of *lys-7(ok1384)*, or *lys-8(ok3504)* mutants, or *lys-2* RNAi worms fed either live *E. coli* OP50 (A) or heat-killed (HK) *E. coli* OP50 (B). **P* < 0.05. ns, not significant. **(C)** Knockdown of *lys-2* by RNAi did not affect the lifespan of *lys-7(ok1384)*; *lys-8(ok3504)* double mutants fed live (C) or HK *E. coli* OP50 (D). ns, not significant. *P*-values throughout were calculated using log-rank test.

**Figure 6-figure supplement 1-source data 1**

**Lifespan assays summary.**

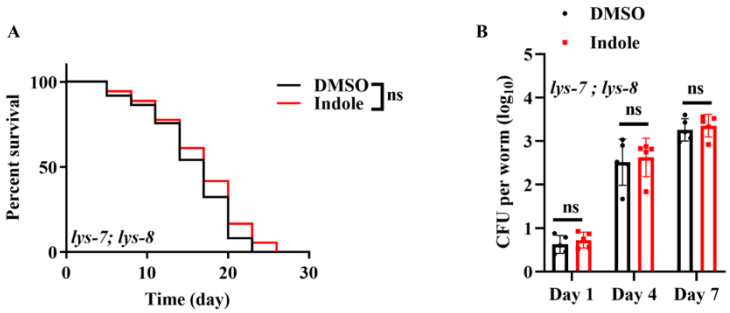


**Figure 6-figure supplement 2. Indole-mediated lifespan extension in worms depends on LYS-7 and LYS-8.**

(**A**) Supplementation with indole (100 μM) no longer extended lifespan in *lys-7(ok1384); lys-8(ok3504)* double mutants. *P*-values throughout were calculated using log-rank test. (**B**) Supplementation with indole failed to suppress the increase the CFU of K-12 in *lys-7(ok1384); lys-8(ok3504)* double mutants. These results are means ± SEM of five independent experiments (n > 30 worms per experiment). ns, not significant. *P*-values were calculated using the unpaired t-test.

**Figure 6-figure supplement 2-source data 1**

**Lifespan assays summary and quantification results.**

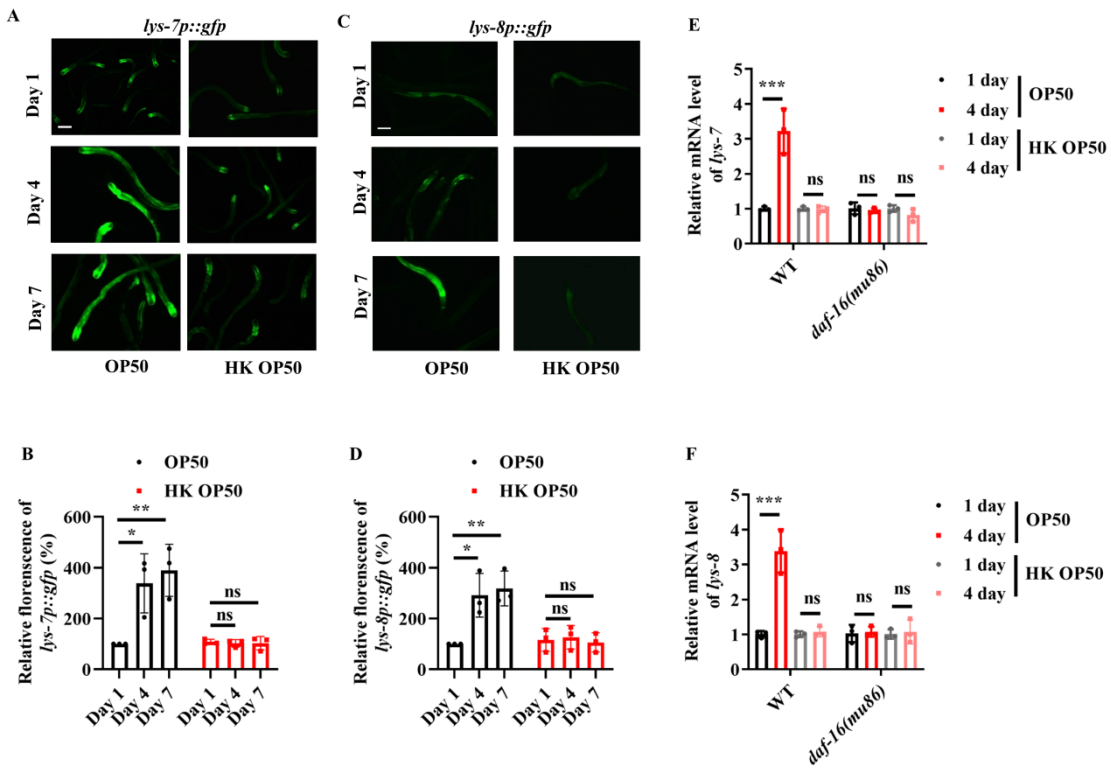


**Figure 7-figure supplement 1. The expressions of *lys-7p::gfp* and *lys-8p::gfp* are up-regulated in worms with age.**

**(A and C)** Representative images of *lys-7p::gfp* (A) and *lys-8p::gfp* (C) in worms fed live *E. coli* OP50. Scale bars: 100 μm. **(B and D)** Quantification of fluorescent intensity of *lys-7p::gfp* (B) and *lys-8p::gfp* (D). The expressions of *lys-7p::gfp* and *lys-8p::gfp* were significantly up-regulated in worms fed live *E. coli* OP50, but not heat-killed (HK) *E. coli* OP50, on Days 4 and 7. These results are means ± SEM of three independent experiments (n > 35 worms per experiment). **P* < 0.05; ***P* < 0.01. **(E and F)** The mRNA levels of *lys-7* (E) and *lys-8* (F) are up-regulated in wild-type (WT) worms fed live *E. coli* OP50, but not HK *E. coli* OP50, on Day 4. These increases in the mRNA levels of *lys-7* (E) and *lys-8* (F) were abolished by a mutation in *daf-16(mu86)*. ****P* < 0.001. These results are means ± SEM of three independent experiments. *P*-values (**B,** and **D-F**) were calculated using the unpaired t-test.

**Figure 7-figure supplement 1-source data 1**

**Quantification results.**

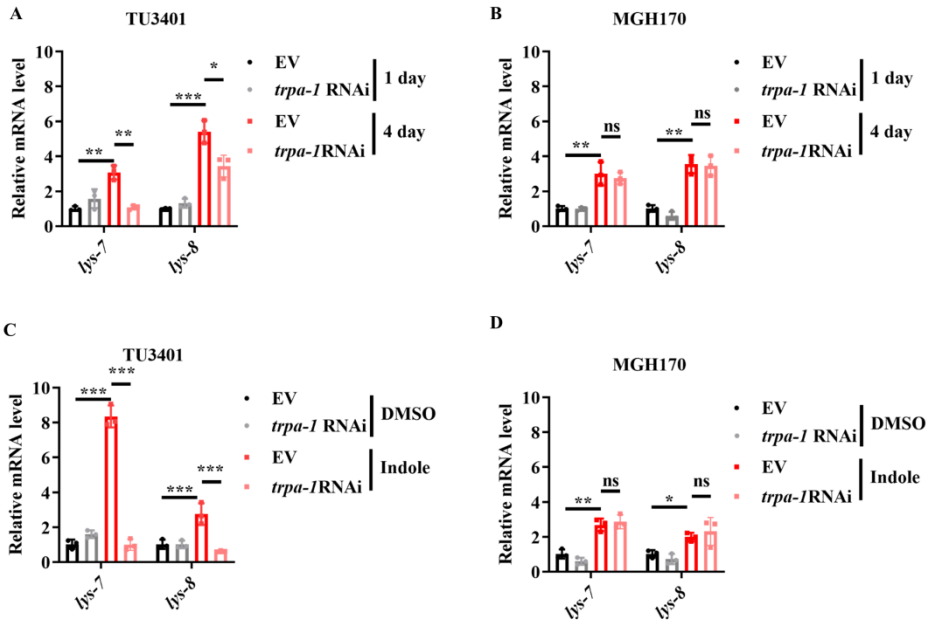


**Figure 7-figure supplement 2. TRPA-1 in neurons is required for the expression *lys-7* and *lys-8*.**

(**A and B**) The mRNA levels of *lys-7* and *lys-8* were significantly down-regulated in worms subjected to neuronal-specific (A), but not intestinal-specific (B), knockdown of *trpa-1* by RNAi. These results are means ± SEM of three independent experiments. ***$P < 0.001$. **$P < 0.01$. *$P < 0.05$. ns, not significant. (**C and D**) Supplementation with indole (100 μM) up-regulated the mRNA levels of *lys-7* and *lys-8* in worms subjected to neuronal -specific (C), but not intestinal -specific (D), knockdown of *trpa-1* by RNAi. These results are means ± SEM of three independent experiments. **$P < 0.01$; ***$P < 0.001$. ns, not significant. *P*-values (**A-D**) were calculated using the unpaired t-test.

**Figure 7-figure supplement 2-source data 1**

**Quantification results.**

| Atom position | $^{1}$H NMR ($\delta_H$) | $^{13}$C NMR ($\delta_c$) |
|---|---|---|
| 1 | - | - |
| 2 | 7.22 (1H, d, $J$ = 3.0 Hz) | 124.0 |
| 3 | 6.44 (1H, d, $J$ = 3.0 Hz) | 100.9 |
| 4 | - | 128.0 |
| 5 | 7.55 (1H, d, $J$ = 7.8 Hz) | 119.8 |
| 6 | 7.00 (1H, t, $J$ = 7.8 Hz) | 120.8 |
| 7 | 7.10 (1H, t, $J$ = 7.8 Hz) | 118.6 |
| 8 | 7.38 (1H, d, $J$ = 7.8 Hz) | 110.7 |
| 9 | - | 136.3 |

**Table S1. The $^{1}$H and $^{13}$C NMR spectroscopic data of indole at 600 MHz for $^{1}$H NMR and 150 MHz for $^{13}$C NMR with reference to the solvent signals.**

NMR spectra of indole were recorded in $CDCl_3$. The corresponding $^{1}$H and$^{13}$C NMR spectra were depicted in **Figure 2-figure supplement 1**, respectively. $\delta_H$ were recorded at 600 MHz and the measured values of $\delta_H$ were in good agree with published NMR data for indole. $\delta_C$ were recorded at 150 MHz and the values exhibited a good consistency with published data in ppm (Yagudaev, 1986).

## References

Yagudaev, M.R. (1986). Application Of H-1 And C-13 Nmr-Spectroscopy In Structural Investigations Of Indole Vinca Alkaloids. Khim Prirodnyk Soedi, 3-15.